Published for SISSA by Springer

Received: *June 7, 2010*
Accepted: *June 29, 2010*
Published: *July 16, 2010*

Holographic Roberge-Weiss transitions

Gert Aarts, S. Prem Kumar and James Rafferty

Department of Physics, Swansea University,
Swansea, SA2 8PP, U.K.

E-mail: g.aarts@swansea.ac.uk, s.p.kumar@swansea.ac.uk, pyjames@swansea.ac.uk

Abstract: We investigate $\mathcal{N} = 4$ SYM coupled to fundamental flavours at nonzero imaginary quark chemical potential in the strong coupling and large N limit, using gauge/gravity duality applied to the D3-D7 system, treating flavours in the probe approximation. The interplay between $\mathbb{Z}_N$ symmetry and the imaginary chemical potential yields a series of first-order Roberge-Weiss transitions. An additional thermal transition separates phases where quarks are bound/unbound into mesons. This results in a set of Roberge-Weiss endpoints: we establish that these are triple points, determine the Roberge-Weiss temperature, give the curvature of the phase boundaries and confirm that the theory is analytic in μ^2 when $\mu^2 \approx 0$.

Keywords: Gauge-gravity correspondence, Lattice QCD, AdS-CFT Correspondence

ArXiv ePrint: 1005.2947

doi:10.1007/JHEP07(2010)056

JHEP07(2010)056

Contents

JHEP07(2010)056

1 Introduction

The duality between strongly interacting gauge theories and gravity, via the AdS/CFT correspondence [1], has fuelled the exploration of a large number of strongly coupled systems and their associated thermodynamic phase structures. Essential features of the thermodynamics of pure gauge theories such as the deconfinement transition at strong coupling are captured by semiclassical gravitational transitions [2, 3]. When applied to $\mathcal{N} = 4$ supersymmetric (SUSY) gauge theory, the gauge/gravity correspondence yields the full phase diagram at strong coupling, as a function of both temperature and chemical potentials for global R-symmetries [4–7]. Various qualitative aspects of this phase diagram are also mirrored by the weakly coupled gauge theory [8–12]. Extensions of such holographic computations to include gauge theories with matter fields transforming in the fundamental

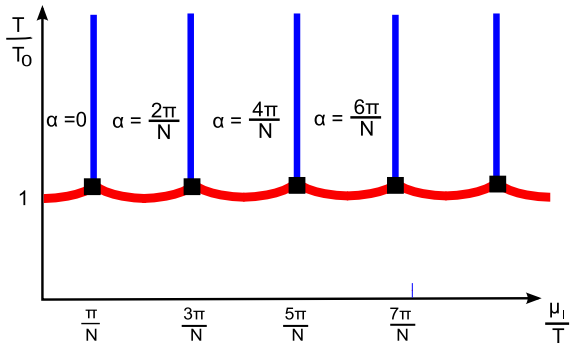

Figure 1. Phase diagram in the plane of temperature T and imaginary quark chemical potential μ_I. The blue lines represent the first order Roberge-Weiss transitions in the high-temperature phase. The red line is the line of first-order phase transitions separating the high- and the low-temperature phases. The Roberge-Weiss endpoints, indicated by the black squares, are triple points at $(\mu_{\rm RW}, T_{\rm RW})$. The phase of the Polyakov loop is denoted with α.

representation of the gauge group have been considered [13–15] and the resulting phase diagrams have been extensively studied by various groups [16–29].

In this paper we study the thermodynamics of the SU(N) $\mathcal{N} = 4$ theory coupled to $\mathcal{N} = 2$ SUSY matter with an *imaginary* chemical potential for quark (flavour) number, using the D3-D7 setup at strong coupling, introduced in [13, 14]. The theory has N_f flavour multiplets preserving $\mathcal{N} = 2$ SUSY, with $N_f \ll N$, so that flavour loops are suppressed in the large-N theory. The physical motivation and rationale behind the investigation of thermodynamics with an imaginary chemical potential μ_I is discussed below; in short, it provides an additional window into the dynamics and phase structure of "QCD-like" gauge theories with fundamental matter fields.

Our study of the gravity dual description of the strongly coupled gauge theory reveals the phase diagram depicted in figure 1. At high temperatures T, there is an infinite sequence of first order transitions at $\mu_I = \mu_{\rm RW}$, where

$$\mu_{\rm RW} \equiv (2r-1)\frac{\pi T}{N}\,, \qquad r \in \mathbb{Z}\,, \tag{1.1}$$

characterized by jumps in the phase of the Polyakov loop order parameter. The quarks, i.e. the fundamental matter degrees of freedom, remain unbound and are represented by the so-called black-hole embeddings of probe D7-branes in the gravity dual setup. The sequence of first order transition lines appears due to the interplay between $\mathbb{Z}_N$-invariance of the adjoint fields and the imaginary quark chemical potential μ_I, as was argued on general grounds by Roberge and Weiss in the context of QCD [30]. It reflects the presence of unbound or deconfined fundamental matter degrees of freedom (carrying non-zero N-ality). A significant feature of the Roberge-Weiss (RW) lines is that they must end at some low temperature, below which quarks are confined or bound, thus acting as a diagnostic for confinement/deconfinement of quarks. The order of the transition at the Roberge-Weiss endpoints depends on the theory in question. In the holographic example we study here, the endpoints are *triple points* since the RW lines meet another line of first order

JHEP07(2010)056

transitions (indicated in red in figure 1) at $T = T_{\rm RW}$. Below this line the quarks are bound into mesons corresponding to fluctuations of the "Minkowski-embeddings" of probe D7-branes in the gravity dual [31]. The line of meson-melting transitions is an extension to imaginary values of the same phenomenon found in this model for real values of the chemical potential [16, 19, 22, 27]. We find that this phase boundary is given by a set of parabola, centered at $\mu_I/T = 2\pi r/N$ ($r \in \mathbb{Z}$). Explicitly, we find

$$\frac{T_c(\mu_I) - T_0}{T_0} = \frac{\kappa}{\lambda}\left(\frac{\mu_I}{T_0} - \frac{2\pi r}{N}\right)^2, \qquad \kappa \approx 43.5, \tag{1.2}$$

when

$$\frac{(2r-1)\pi}{N} < \frac{\mu_I}{T} < \frac{(2r+1)\pi}{N}. \tag{1.3}$$

Here $T_0 = T_c(\mu_I = 0)$ is the critical temperature for vanishing μ_I and $\lambda = g^2_{\rm YM}N$ is the 't Hooft coupling, which is taken to be large. The Roberge-Weiss endpoints are therefore located at $(\mu_{\rm RW}, T_{\rm RW})$, where $\mu_{\rm RW}$ is given by eq. (1.1) and

$$\frac{T_{\rm RW}}{T_0} = 1 + \frac{\kappa}{\lambda}\frac{\pi^2}{N^2}\,. \tag{1.4}$$

The meson melting temperature at zero chemical potential is determined by the typical meson mass scale M in this model and $T_0 \approx 0.77M$, where $M = 2m_q/\sqrt{\lambda}$ with m_q the common mass of the $\mathcal{N} = 2$ flavour multiplets [27, 31].

Since the flavour degrees of freedom are probes in the large-N theory, they do not affect the dynamics of the adjoint degrees of freedom of $\mathcal{N} = 4$ SYM, which remain deconfined at all temperatures. Hence, the low-temperature phase does not resemble the gluon sector of QCD. However, fundamental matter in this system is bound into mesonic states at low temperature and unbound at high temperature (with the scale set by the meson mass). A notion of a low- and a high-temperature phase therefore still exists.

The primary motivation for the exploration of thermodynamics in the presence of imaginary chemical potentials comes from QCD. As is well known, the phase structure of QCD at nonzero temperature and quark chemical potential is difficult to determine. At large temperature and/or chemical potential predictions can be made with perturbation theory, due to asymptotic freedom, but most of the phase diagram requires a nonperturbative evaluation. Thermal properties ($T > 0$) at vanishing chemical potential ($\mu = 0$) are being investigated vigorously using lattice QCD; for a recent review, see e.g. [33]. At non-zero chemical potential however, a straightforward application of lattice QCD runs into problems. Since the fermion determinant is complex, algorithms based on importance sampling can no longer be applied, resulting in the infamous sign problem. Various approaches to circumvent the sign problem in QCD at finite density have been developed over the past decade; an up-to-date review can be found in [34].

The sign problem is due to the nonhermiticity of the Dirac operator. Let $\not{D}$ denote the massless Dirac operator, satisfying $\gamma_5 \not{D} \gamma_5 = \not{D}^\dagger$. Integrating out the fermion fields then yields the determinant $\det M(\mu) = \det(\not{D} + m + \mu\gamma_0)$. Using γ_5-hermiticity it immediately follows that this determinant is complex,

$$[\det M(\mu)]^* = \det M(-\mu^*), \tag{1.5}$$

JHEP07(2010)056

unless the chemical potential vanishes or is purely imaginary. This last observation suggests that lattice QCD simulations at imaginary chemical potential $\mu = i\mu_I$ can be performed using standard algorithms. Information about the phase structure at real chemical potential can then be obtained by analytic continuation: since the partition function is an even function of μ, analytical continuation from imaginary μ ($\mu^2 < 0$) to real μ ($\mu^2 > 0$) is in principle straightforward. This approach has indeed been used extensively [35–45].

As mentioned above, the phase structure at nonzero imaginary chemical potential is nontrivial due to the interplay between the $\mathbb{Z}_N$ symmetry and μ_I [30]. As we will review below, the partition function is periodic in μ_I and satisfies

$$Z[\mu_I] = Z\left[\mu_I + \frac{2\pi r T}{N}\right], \qquad r \in \mathbb{Z}. \tag{1.6}$$

Combined with reflection symmetry $Z[\mu_I] = Z[-\mu_I]$, this leads to Roberge-Weiss transitions at $\mu_I = \mu_{\rm RW}$ (eq. (1.1)). At these values of μ_I, the theory undergoes a transition between adjacent $\mathbb{Z}_N$ sectors, which can be distinguished by the phase of the Polyakov loop.

At high temperature the Roberge-Weiss transitions are first order, resulting in non-analytic behaviour of observables at $\mu_I = \mu_{\rm RW}$. At low temperature, the Roberge-Weiss periodicity is smoothly realized and no nonanalyticity is present. This was first suggested in [30] and has been confirmed with lattice QCD simulations [35–45]. The Roberge-Weiss lines therefore end. In QCD the high- and low-temperature phase are separated by a thermal confinement/deconfinement transition,[1] which extends into the μ_I direction. It is widely assumed that this transition line will join the Roberge-Weiss lines at $\mu_I = \mu_{\rm RW}$. Generically the phase diagram will therefore be as depicted in figure 1.

In QCD properties of the confinement/deconfinement transition depend crucially on the number of flavours and the quark masses. For instance, for three degenerate flavours, the transition is first order for light and heavy quarks (which is tied to the chiral and centre symmetries respectively), while for intermediate quark masses, the transition is a crossover. It has only recently been demonstrated that the Roberge-Weiss endpoint is a triple point for two [43] and three [38] degenerate light or heavy flavours, while it is a second order endpoint in the 3d Ising universality class for intermediate quark masses. Moreover, in a beautiful paper [38], de Forcrand and Philipsen argued in the case of heavy quarks that the tricritical point found in the quark mass-temperature plane at $\mu_I = \mu_{\rm RW}$ dictates the deconfinement critical line for real μ by tricritical scaling.

It is therefore clear that an understanding of the phase diagram at imaginary chemical potential can provide important insight into the phase structure at real chemical potential. For this reason this topic has been under intense investigation, using both lattice QCD as mentioned above, renormalization-group studies [46], as well as effective models [47–50]. In this paper we take a third approach and apply gauge-gravity duality to study the phase diagram of a strongly coupled gauge theory at imaginary chemical potential.

This paper is organized as follows. We begin by reviewing the arguments of [30] in section 2 and summarize results that can be obtained at arbitrarily weak gauge coupling.

[1] Although strictly speaking it is only a confinement/deconfinement transition when the quarks are infinitely heavy, we use this terminology for light quarks as well.

JHEP07(2010)056

In section 3 we review the well known properties of the gauge theory model we consider ($\mathcal{N}=4$ SYM coupled to $\mathcal{N}=2$ matter). Section 4 contains the holographic description of the model at imaginary chemical potential and a numerical study of the configurations that dominate the ensemble as a function of temperature and μ_I. The resulting phase diagram is constructed in section 5. Section 6 contains a brief outlook. In the appendix we outline, in some detail, the thermodynamics of the model at weak coupling.

2 Roberge-Weiss phase transitions

It is well known that the deconfinement phase transition in SU(N) gauge theories without matter in the fundamental representation can be precisely characterized, in the Euclidean formulation, by the expectation value of the thermal Wilson line or Polyakov loop $P = \frac{1}{N}\mathrm{Tr}\exp(i\oint A_\tau)$. The $\mathbb{Z}_N$ symmetry of the pure gauge theory under which $P \to Pe^{2\pi ik/N}$, $(k = 0, 1, 2, \ldots N-1)$ is spontaneously broken by an expectation value for the Polyakov loop in the high temperature deconfined phase. This distinction between confining and deconfined phases is lost upon the introduction of matter in the fundamental representation of the gauge group since there is no $\mathbb{Z}_N$ symmetry and the operator P can obtain an expectation value at all temperatures. However, as was argued in [30], there is a remnant of this symmetry which can still be used to distinguish between the phases in which quarks are confined or deconfined.

The idea of [30] is that in theories with fundamental matter and an appropriately defined baryon number U(1)$_B$ symmetry, the difference between the confined and deconfined phases can manifest itself in the behaviour of the theory as a function of an *imaginary* chemical potential for baryon or quark number. With an imaginary chemical potential μ_I for quark number, the thermal partition function

$$Z[\mu_I] = \mathrm{Tr}\left(e^{-\beta H + i\beta\mu_I N_q}\right) \tag{2.1}$$

is naturally periodic under $\mu_I \to \mu_I + 2\pi T$ ($\beta \equiv 1/T$), since N_q is quantized. Hence $\frac{\mu_I}{T} \in [-\pi, \pi]$.

There is a further periodicity of this partition function following from the $\mathbb{Z}_N$ symmetry of the adjoint degrees of freedom [30] and it can be understood as follows. We recall that the (imaginary) chemical potential for fermion number couples to fundamental matter fields in the same way as the time component A_τ of the SU(N) gauge field. The imaginary chemical potential μ_I is introduced by the replacement $\partial_\tau + iA_\tau \to \partial_\tau + iA_\tau - i\mu_I$, acting on matter fields in the fundamental representation.

This μ_I-dependence at the level of the action can be removed by a phase redefinition of fields ϕ charged under U(1)$_B$, and transferred into boundary conditions around the thermal circle,

$$\phi(\vec{x}, \beta) = \pm e^{i\mu_I/T}\,\phi(\vec{x}, 0), \tag{2.2}$$

where the + and − signs apply to bosonic and fermionic modes respectively. We can perform a second variable change, corresponding to a gauge transformation by an element U$(\vec{x}, \tau)$ of SU(N), with the property U$(\vec{x}, \beta) = e^{2\pi ir/N}$ U$(\vec{x}, 0)$, $r \in \mathbb{Z}$. This leaves the action

and the path integral measure invariant, whilst only altering the boundary conditions for the fields around the thermal circle,

$$\phi(\vec{x},\beta) = \pm e^{i\mu_I/T}\, e^{i2\pi r/N}\, \phi(\vec{x},0). \tag{2.3}$$

Since the partition function is left invariant by variable changes, we conclude that

$$Z[\mu_I] = Z\left[\mu_I + \frac{2\pi r T}{N}\right], \qquad r \in \mathbb{Z}. \tag{2.4}$$

This implies that $\frac{\mu_I}{T} \in [-\frac{\pi}{N}, \frac{\pi}{N}]$.

At high temperatures, when the weak coupling approximation is consistent, a perturbative evaluation of the free energy $F[\mu_I] = -\ln[Z]/\beta$ shows first-order phase transitions as a function of μ_I at $\mu_I = \mu_{\rm RW} = (2r-1)\pi T/N$ ($r \in \mathbb{Z}$). These are the Roberge-Weiss transitions. At low temperatures, when the theories are typically strongly coupled, lattice studies suggest that $F[\mu_I]$ is a smooth function of μ_I/T. The situation at very high and very low temperatures is therefore expected to be qualitatively as in figure 1. The nature of the transition between these two behaviours depends on the detailed dynamics of the theories in question, as we have already discussed in the Introduction.

2.1 Roberge-Weiss transitions at weak coupling

At suitably high temperatures when the gauge theory is in a deconfined phase it is generically possible to compute the effective potential as a function of μ_I perturbatively [51, 52]. The details of this calculation at the one-loop level are summarized in the appendix. Here we state the result of this calculation. The basic idea involves computing an effective potential for the eigenvalues of the holonomy around the thermal circle (the Polyakov loop matrix), $\exp(i\oint A_\tau)$ in the presence of fundamental matter. The effective potential at one-loop is the sum of a gluonic (adjoint matter) piece and a flavour (fundamental matter) piece. While the gluonic contribution, V_A, is $\mathbb{Z}_N$ invariant and independent of μ_I, the terms arising from the flavour fields, V_f, are not $\mathbb{Z}_N$ invariant and explicitly depend on the imaginary chemical potential,

$$V_{\rm eff}(\,\{\alpha_i\}\,) = V_A\,(\,\{\alpha_{ij}\}\,) + V_f(\,\{\alpha_i - \mu_I/T\}\,)\,, \qquad \alpha_{ij} \equiv \alpha_i - \alpha_j. \tag{2.5}$$

Here $e^{i\alpha_j}$, $j = 1, 2, \ldots N$ are the eigenvalues of the Polyakov loop matrix. Generically, at high temperatures, in the absence of fields in the fundamental of SU(N), V_A will have N minima, each of which breaks the $\mathbb{Z}_N$ symmetry spontaneously. At these minima $\alpha_i = 2\pi k/N$ for $k = 0, 1, 2, \ldots N-1$. Introduction of fundamental matter turns these into local minima with a single global minimum at $\alpha_i = 0$ for vanishing μ_I. Since V_f depends only on the combination $(\alpha_i - \mu_I/T)$, the global minimum will move to $\alpha_i = 2\pi r/N$ when $\mu_I/T = 2\pi r/N$ ($r \in \mathbb{Z}$). We conclude that the different local minima of the effective potential compete as μ_I is varied and there are first order phase transitions between two neighbouring minima whenever $\mu_I/T = (2r-1)\pi/N$ ($r \in \mathbb{Z}$). The perturbative result for the free energy across these transitions is computed in the appendix. We quote the result here, specifically for a large-N gauge theory coupled to both adjoint and fundamental

JHEP07(2010)056

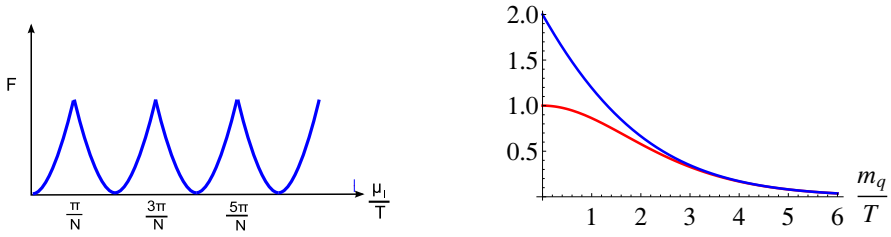

Figure 2. *Left*: The generic behaviour of the free energy across Roberge-Weiss transitions. *Right:* The functions $f_{\rm bose}$ (blue) and $f_{\rm fermi}$ (red) versus the ratio m_q/T.

matter fields. For such a theory with n_f complex scalars and $\tilde{n}_f$ Weyl fermions, all in the fundamental representation of SU(N) and with mass m_q, we find the free energy as a function of μ_I to be

$$F[\mu_I] = N\,\frac{T^4}{12}\left[n_f\, f_{\rm bose}\left(\frac{m_q}{T}\right) + \tilde{n}_f\, f_{\rm fermi}\left(\frac{m_q}{T}\right)\right] \min_{r\in\mathbb{Z}}\left(\frac{\mu_I}{T} - \frac{2\pi r}{N}\right)^2, \tag{2.6}$$

where

$$f_{\rm bose}\,(x) = \frac{3}{2\pi^2}\int_0^\infty y^2\,dy\,\frac{1}{\sinh^2\left(\frac{1}{2}\sqrt{y^2+x^2}\right)}, \tag{2.7}$$

and

$$f_{\rm fermi}\,(x) = \frac{3}{2\pi^2}\int_0^\infty y^2\,dy\,\frac{1}{\cosh^2\left(\frac{1}{2}\sqrt{y^2+x^2}\right)}. \tag{2.8}$$

These functions are determined by the Bose-Einstein and Fermi-Dirac distributions for free particles. As $m_q/T \to 0$, $f_{\rm bose}$ and $f_{\rm fermi}$ approach 2 and 1 respectively.

The free energy is a function with cusps (figure 2) located at odd integer multiples of π/N where phase transitions occur. It is a quadratic function only because we chose to look at the large-N limit which forces the Roberge-Weiss transition points to be closely spaced within intervals of $2\pi/N$. Hence only the second derivative of the free energy function at its minimum is relevant. The strength of the transition, as measured by the coefficient functions $f_{\rm bose}$ and $f_{\rm fermi}$ varies with the ratio m_q/T. We have plotted these in figure 2. Notable features are their behaviours for small and large masses. $f_{\rm bose}$ is determined by the Bose-Einstein distribution which diverges for small masses and is responsible for the linear dependence on m_q/T when $m_q \ll T$. For large masses (or low temperatures), both coefficients are exponentially Boltzmann-suppressed.

We note here that at weak coupling only the ratio m_q/T is relevant. Typically however, nonperturbative physics will generate another scale (such as $\Lambda_{\rm QCD}$ in QCD). In that case the notion of high and low temperatures and masses has an independent meaning and the weak coupling result can be trusted when $T \gg \Lambda_{\rm QCD}$. In the model we study in this paper, the 't Hooft coupling $\lambda = g^2_{\rm YM}N$ can be dialled to any fixed value (assuming the number of flavours is small compared to N), and there is no dynamical scale. This means that the ratio m_q/T is the only parameter which can be varied at fixed 't Hooft coupling and we expect the above picture to be valid for $\lambda \ll 1$. For large λ, the perturbative evaluation is clearly not valid and we must use the dual gravity picture.

JHEP07(2010)056

3 $\mathcal{N} = 4$ theory coupled to $\mathcal{N} = 2$ flavours

We will consider the $\mathcal{N} = 4$ theory in flat space, and at finite temperature , coupled to $\mathcal{N} = 2$ supersymmetric matter transforming in the fundamental representation of the SU(N) gauge group. When the number, N_f, of $\mathcal{N} = 2$ hypermultiplets is small ($N_f \ll N$), the effect of these hypermultiplets on the dynamics of the $\mathcal{N} = 4$ matter (such as the running of the gauge coupling) can be consistently neglected and the matter fields can be treated in a "probe" approximation. The $\mathcal{N} = 4$ degrees of freedom are always in the deconfined phase at finite temperature in flat space. This particular theory can be readily studied at strong coupling using the AdS/CFT correspondence as was first pointed out in [13, 14].

3.1 The classical theory

The $\mathcal{N} = 4$ theory can be naturally coupled to matter in the fundamental representation and thereby preserve a maximum of eight supercharges ($\mathcal{N} = 2$ SUSY). In the language of $\mathcal{N} = 1$ superfields, the $\mathcal{N} = 2$ hypermultiplet consists of two chiral superfields $(Q, \tilde{Q})$ transforming in the $(\bar{N}, N)$ representation of the SU(N) gauge group. The superfields in the hypermultiplet each consist of a squark and a quark (q, ψ) and $(\tilde{q}, \tilde{\psi})$.

Introducing N_f hypermultiplets $(Q^i, \tilde{Q}_i)$ and using the $\mathcal{N} = 1$ SUSY notation, the superpotential of the theory with flavours can be written as

$$W = \frac{1}{g^2_{\rm YM}} \left(\sum_{i=1}^{N_f} \left(\sqrt{2}\, \tilde{Q}_i\, \Phi_3\, Q^i + m_q\, \tilde{Q}_i\, Q^i \right) + \sqrt{2}\, {\rm Tr}(\Phi_3\, [\Phi_1, \Phi_2]) \right). \tag{3.1}$$

The three adjoint chiral multiplets of the $\mathcal{N} = 4$ theory are Φ_1, Φ_2 and Φ_3. After coupling to the $\mathcal{N} = 2$ hypermultiplets, Φ_3 naturally becomes the scalar part of the $\mathcal{N} = 2$ vector multiplet, while $\Phi_{1,2}$ together constitute an $\mathcal{N} = 2$ adjoint hypermultiplet. Note that while it is possible to introduce distinct masses for each of the N_f flavours in question, we will only consider the case where all masses are equal. For equal quark masses the theory has a $\mathrm{U}(N_f) \simeq \mathrm{U}(1)_B \times \mathrm{SU}(N_f)$ flavour symmetry group. The $\mathrm{U}(1)_B$ is identified as the "baryon number" symmetry[2] under which Q^i and $\tilde{Q}_i$ transform with equal and opposite charges. At the level of the Lagrangian, the mass term for the hypermultiplet induces the operator,

$$\mathcal{L} \supset \frac{1}{g^2_{\rm YM}} \left(m_q\, \tilde{\psi}^i \psi_i + m_q^2 q_i^\dagger q^i + m_q^2 \tilde{q}_i^\dagger \tilde{q}^i + \sqrt{2} m_q q_i^\dagger \Phi_3 q^i + + \sqrt{2} m_q \tilde{q}_i \Phi_3 \tilde{q}^{i\dagger} + \text{h.c.} \right). \tag{3.2}$$

In what follows, the expectation value of the operator $\Sigma_m \equiv \frac{\partial \mathcal{L}}{\partial m_q}$ will be referred to as the "quark condensate".

3.2 D-brane picture

At weak coupling (and zero temperature) in the D-brane picture in type IIB string theory, the $\mathcal{N} = 2$ matter hypermultiplets can be introduced by placing N_f coincident D7-branes

[2] For massless quarks the theory has the global symmetry group, $\mathrm{U}(1)_B \times \mathrm{SU}(N_f) \times \mathrm{SU}(2)_R \times \mathrm{U}(1)_R \times \mathrm{SU}(2)_\Phi$. The $\mathrm{SU}(2)_R \times \mathrm{U}(1)_R$ factor is the R-symmetry group of the $\mathcal{N} = 2$ gauge theory.

JHEP07(2010)056

in the presence of N coincident D3-branes. The low energy dynamics of the latter is $\mathcal{N}=4$ SUSY gauge theory. The D3 and D7-brane worldvolumes span the coordinates indicated below in the ambient ten dimensional spacetime,

Coordinates	x_0	x_1	x_2	x_3	x_4	x_5	x_6	x_7	x_8	x_9
D3	×	×	×	×						
D7	×	×	×	×	×	×	×	×		

The fluctuations of the open strings stretching between the D3 and D7-branes yield the N_f hypermultiplets transforming in the fundamental representation of the SU(N) gauge symmetry of the D3-branes. These also transform under the $\mathrm{U}(N_f) \simeq \mathrm{U}(1)_B \times \mathrm{SU}(N_f)$ symmetry group associated to the D7's, which appears as a flavour symmetry at low energies. The separation in the x_8-x_9 plane, between the stack of D3-branes and the flavour branes translates to a mass m_q for the hypermultiplets. For a separation ℓ in this plane, the hypermultiplet mass is given by the string tension times the separation, $m_q = \frac{\ell}{2\pi\alpha'}$.

4 Thermodynamics at strong coupling

In the large-N and strong 't Hooft coupling limit ($\lambda = g^2_{\mathrm{YM}} N \gg 1$), the fundamental hypermultiplets are introduced as probe D7-branes into the geometry sourced by the N D3-branes, namely $AdS_5 \times S^5$ [13, 14]. At finite temperature, in the deconfined phase, the corresponding geometry is the Schwarzschild black hole in $AdS_5 \times S^5$ (with flat horizon). Wick rotating to Euclidean signature, the spacetime metric is

$$ds^2 = \left(f(r) d\tau^2 + \frac{dr^2}{f(r)} + \frac{r^2}{R^2} d\vec{x}^2 + R^2\, d\Omega_5^2 \right), \tag{4.1}$$

where

$$f(r) = \frac{1}{R^2}\left(r^2 - \frac{r_H^4}{r^2} \right), \qquad r_H = \pi T R^2, \qquad R^4 = 4\pi (g_s N) \alpha'^2 = g^2_{\mathrm{YM}} N\, \alpha'^2\,, \tag{4.2}$$

and R is the AdS radius.

In the Euclidean picture the geometry ends smoothly at $r = r_H$, provided we make the periodic thermal identification $\tau \simeq \tau + 1/T$. Topologically, the Euclidean black hole spacetime is $\mathbb{R}^3 \times D_2 \times S^5$.

As suggested by the weak coupling setup in section (3.2), the flavour D7-branes must wrap an $S^3 \subset S^5$ while filling the AdS_5 directions [13, 14, 16]. The embedding of the D7-brane is characterized by the "slipping angle" which determines the size of the three-sphere wrapped by the D7-brane. The slipping angle θ is defined by the following paramerization of the S^5 metric

$$d\Omega_5^2 = d\theta^2 + \sin^2\theta\, d\phi^2 + \cos^2\theta\, d\Omega_3^2\,; \qquad 0 \le \theta \le \frac{\pi}{2}\,. \tag{4.3}$$

It is more convenient to rewrite the background metric in a Fefferman-Graham type coordinate system [53, 54]. We use the conventions of [22], to write the black hole metric in

the form

$$ds^2 = \frac{1}{2}\frac{\rho^2}{R^2}\left(\frac{h^2}{\tilde{h}}\,d\tau^2 + \tilde{h}\,d\vec{x}^2\right) + \frac{R^2}{\rho^2}\left(d\rho^2 + \rho^2\,d\Omega_5^2\right), \tag{4.4}$$

$$h(\rho) \equiv 1 - \frac{r_H^4}{\rho^4}, \qquad \tilde{h}(\rho) \equiv 1 + \frac{r_H^4}{\rho^4}.$$

This form of the metric is obtained after the coordinate change $r^2 = \frac{1}{2}\left(\rho^2 + r_H^4/\rho^2\right)$, and we take the metric of the five-sphere as in eq. (4.3). The slipping angle θ will be dual to the quark mass operator Σ_m, and depend only on the radial coordinate of AdS space,

$$\theta = \theta(\rho). \tag{4.5}$$

This parametrization is convenient for making contact with the weak coupling D-brane picture. Focussing on the six directions transverse to the D3-branes, we write

$$d\rho^2 + \rho^2 d\Omega_5^2 = d\rho_2^2 + \rho_2^2\,d\phi^2 + d\rho_1^2 + \rho_1^2\,d\Omega_3^2, \tag{4.6}$$

with

$$\rho_1 = \rho\cos\theta, \qquad \rho_2 = \rho\sin\theta. \tag{4.7}$$

The $x_8 - x_9$ plane can now be identified with the (ρ_2, ϕ) plane. We choose the D7-brane to be at $\phi = 0$, i.e. the x_8 axis. The asymptotic value of the D3-D7 separation, given by ρ_2 for large ρ, yields the hypermultiplet mass m_q.

4.1 $\mathbb{Z}_N$ breaking in thermal $\mathcal{N} = 4$ theory

As argued in [55], one may understand the spontaneous breaking of the $\mathbb{Z}_N$ center symmetry at high temperatures as follows . We first note that the disk D_2 in the black hole geometry naturally allows turning on a Neveu-Schwarz potential B with $dB = 0$ and

$$\alpha \equiv \frac{1}{2\pi l_s^2}\int_{D_2} B. \tag{4.8}$$

This yields a phase $e^{i\alpha}$ for the Polyakov-Maldacena loop[3] [56, 57] computed by wrapping a fundamental string worldsheet on the cigar D_2. Thus α is defined modulo 2π. One then finds that an effective potential for α is induced if we consider terms in the type IIB effective action that depend on the RR 3-form $F_{(3)}$,

$$S_{\rm IIB} \supset \frac{1}{(2\pi)^7 l_s^8}\left(\int d^{10}x\,\sqrt{g}\,\frac{1}{12}F_{(3)}^2 - \int F_{(5)}\wedge F_{(3)}\wedge B\right). \tag{4.9}$$

[3]Strictly speaking, the Wilson loop computed by the wrapped string world-sheet is the supersymmetric version of the standard Polyakov loop and includes the adjoint scalar fields of $\mathcal{N} = 4$ SYM in its definition, $\mathcal{U} \equiv \exp i\oint(A_\tau - i\theta^I(\tau)\Phi^I)$. This is an important distinction in principle, but will not influence our discussion below, as the Polyakov-Maldacena loop has the same transformation properties under $\mathbb{Z}_N$ transformations as the standard Polyakov loop order parameter.

JHEP07(2010)056

Integrating over $S^5 \times D_2$, we may obtain the effective theory for the $F_{(3)}$ field on $\mathbb{R}^3$. Since $F_{(3)}$ has only one non-zero component F_{123} on $\mathbb{R}^3$ we have

$$S_{\text{eff}}[F_{(3)}] = \int d^3x \left[\frac{\lambda}{T^3} \frac{1}{2^8 \pi^6 l_s^4} (F_{123})^2 - \frac{N\alpha}{4\pi^2 l_s^2} F_{123} \right], \tag{4.10}$$

where we have used the fact that the type IIB background has N units of five-form flux through S^5, $\int_{S^5} F_5/(2\pi l_s)^4 = N$. Adapting the arguments arising in the context of U(1) gauge theory in two dimensions to the present situation [55], gauge invariance of quantum states implies the quantization of F_{123}. States are characterized by a constant (quantized) value for the field strength (similarly to constant electric fields in two dimensions) and one finally finds the effective potential for the phase of Polyakov-Maldacena loop to be

$$V_A(\alpha) = 4\pi^2 N^2 T^4 \frac{1}{\lambda} \min_{r \in \mathbb{Z}} \left(\alpha - \frac{2\pi}{N} r \right)^2. \tag{4.11}$$

The potential is minimized when $\alpha = 2\pi r/N$ for $r \in \mathbb{Z}$ and this leads to a spontaneous breaking of the $\mathbb{Z}_N$ symmetry of the $\mathcal{N} = 4$ theory in the deconfined, high temperature phase. Note that this effective potential is $\mathcal{O}(N^2)$, as expected for a leading order large-N effect and proportional to T^4, as expected from dimensional analysis. Interestingly, it is also proportional to $1/\lambda$ in the strongly coupled theory.

4.2 The effect of flavours

Now we would like to calculate how the effective potential for α is modified upon introducing fundamental flavours and in the presence of an *imaginary* chemical potential for quark number. The basic effect of introducing flavour D7-branes was already addressed in [58] and was argued to lift the degeneracy of the N vacua discussed above. The overall dynamics of N_f flavour D7-branes, ignoring the non-Abelian world-volume degrees of freedom in the probe limit ($N_f \ll N$), can be described by the (Euclidean) Dirac-Born-Infeld action

$$S_{D7} = N_f T_{D7} \int d^8\xi e^{-\Phi} \sqrt{\det(^*g + (2\pi\alpha' F + {}^*B))}, \tag{4.12}$$

where $^*g$ and $^*B$ are the pullbacks of the spacetime metric and the Neveu-Schwarz two-form potential on to the D7-brane worldvolume. In addition we have that the dilaton $e^{-\Phi} = 1$ in the background dual to the $\mathcal{N} = 4$ SUSY gauge theory. The D7-brane tension can be written in terms of gauge theory parameters λ, N (and R, the AdS radius) as

$$T_{D7} = \frac{1}{g_s \alpha'^4 (2\pi)^7} = \frac{\lambda N}{32\pi^6 R^8}. \tag{4.13}$$

We will take the D7-brane probe to wrap the S^3 in eq. (4.3) at an angle θ and fill the directions $\tau, \vec{x}$ and ρ. For the most part, we will primarily be interested in classical configurations that completely wrap D_2, the cigar in the Euclidean black hole, corresponding to "melted meson" states [19, 22]. For these configurations it will be consistent to turn on a field strength F along the world-volume. A real value for F in the Euclidean action will correspond to an imaginary gauge potential upon Wick rotating back to Lorentzian signature.

JHEP07(2010)056

4.3 Imaginary chemical potential

In the boundary field theory formulated on Minkowski space, a chemical potential for a global U(1) symmetry can be thought of as follows: We imagine that the global symmetry is gauged and then turn on a constant background value for the time component of the gauge field, while setting other components to zero. A real chemical potential is obtained by assigning an imaginary constant value for this background gauge field in the Euclidean formulation. Equivalently, to get *imaginary* chemical potential for the $U(1)_B$ global symmetry, in the Euclidean theory we must introduce a real value for the time component of the background gauge field associated to $U(1)_B$. This is very natural in the AdS/CFT framework.

The gauge field associated to the overall U(1) factor describing the center-of-mass dynamics of the probe D7-branes, is dual to $U(1)_B$. In the Euclidean theory, the imaginary chemical potential μ_I corresponds to a constant real boundary value for the gauge field A_τ on the world-volume of the D7-brane,

$$\mu_I = -T \int_0^\beta d\tau \int_{r_H}^\infty d\rho \, F_{\tau\rho} = \lim_{\rho\to\infty} A_\tau(\rho). \tag{4.14}$$

Here we choose the gauge freedom to set $A_\rho = 0$ and we require that $A_\tau(r_H) = 0$ in order to avoid a singularity at the tip of the cigar. We are implicitly assuming that the D7-brane wraps the black hole cigar D_2 completely. The case where it turns back before getting to the horizon will be discussed separately.

The action for the D7-brane probe configuration described above is

$$S_{D7} = 2\pi^2 N_f T_{D7} \int \beta \, d^3x \int_{r_H}^\infty d\rho \left(\frac{\rho^3}{4} h \tilde{h} \cos^3\theta \sqrt{1 + \rho^2\theta'(\rho)^2 + 2(2\pi\alpha' F_{\tau\rho} + {}^*B_{\tau\rho})^2 \frac{\tilde{h}}{h^2}} \right). \tag{4.15}$$

We note that in the absence of a B field in the background, this is the same action used in [22], provided we make the replacement $F \to iF$. The qualitative nature of the family of solutions is, however, different to that encountered in [22] for real baryon number chemical potential.

4.3.1 Periodicity in μ_I

The periodicity in μ_I discussed earlier is naturally built into the supergravity dual because the D-brane action only depends on the combination $B + 2\pi\alpha' F$. This means that the classical solutions to the DBI equations of motion will be charactarized by the combination

$$\alpha - \frac{\mu_I}{T} = \int_{D_2} \left(F + \frac{B}{2\pi\alpha'} \right). \tag{4.16}$$

A shift of μ_I by $2\pi T$ can be absorbed by $\alpha \to \alpha + 2\pi$. Hence μ_I is only defined modulo $2\pi T$ as expected from general considerations.

As at weak coupling, there is a further periodicity visible in the finite temperature theory at strong coupling. The shift $\mu_I \to \mu_I + 2\pi T/N$ can be compensated by a corresponding shift of α by the same amount, leaving the physics unchanged since the "glue"

JHEP07(2010)056

sector of the theory ($\mathcal{N}=4$ matter) is invariant under such shifts of α (from eq. (4.11)). Note that this "periodicity" involves a jump from one $\mathbb{Z}_N$ vacuum to another. Therefore, this system should be expected to display the infinite sequence of Roberge-Weiss transitions as the effective potential will be a sum of two pieces, one of which is $\mathbb{Z}_N$ invariant, while the other piece, induced by the fundamental flavours, depends only on the combination $\alpha - \mu_I/T$.

4.4 Solving the DBI equations of motion

The solutions of the D3/D7 system at finite temperature, with and without a *real* chemical potential, have been extensively studied in earlier works [16–24, 26, 32]. Our aim, however, is to study the solutions arising in the presence of the imaginary chemical potential $\mu_I \neq 0$. These will be distinct from the ones found, for example, in [22, 23, 26]. Specifically, for a real chemical potential, the term under the square root in eq. (4.15) would be of the form $\sqrt{1+\rho^2\theta'^2 - 2(2\pi\alpha' F)^2\tilde{h}/h^2}$, yielding solutions with different behaviour to the ones we will find below.

From the solutions to the DBI equations of motion following from eq. (4.15), we will reconstruct the dependence of the effective potential on $\alpha - \mu_I/T$, for generic quark masses.

We work in the gauge $A_\rho = 0$, so that $F_{\tau\rho} = -\partial_\rho A_\tau$. Since the action (4.15) does not depend explicitly on A_τ, the conjugate momentum is conserved. In the usual situation with real chemical potentials, the variable conjugate to A_τ is the quark density. We will continue to refer to this conjugate variable as the "charge density" d, in the situation with an imaginary chemical potential,

$$d \equiv -\frac{\partial \mathcal{L}_{\rm D7}}{\partial A'_\tau} = 2\pi^2 N_f T_{D7} (2\pi\alpha') \frac{\rho^3}{2}\frac{\tilde{h}^2}{h}\cos^3\theta \frac{2\pi\alpha' F_{\tau\rho} + B_{\tau\rho}}{\sqrt{1+\rho^2\theta'^2 + 2(2\pi\alpha' F_{\tau\rho} + B_{\tau\rho})^2 \frac{\tilde{h}}{h^2}}}. \quad (4.17)$$

This is a constant of motion. It is useful to define the dimensionless combination

$$\tilde{d} \equiv d\,(2\pi\alpha')^{-1}\left(2\pi^2 N_f T_{D7}\, r_H^3\right)^{-1} = \frac{8}{\sqrt{\lambda}\, N_f\, N}\frac{d}{T^3}. \quad (4.18)$$

The solutions can be characterized by this dimensionless density which, as we will see below, is restricted to take values less than unity. Solving algebraically for the combination $(2\pi\alpha' F + B)$, using the above equations we obtain

$$B_{\tau\rho} + 2\pi\alpha' F_{\tau\rho} = \tilde{d}\,\frac{2h\sqrt{1+\rho^2\theta'(\rho)^2}}{\sqrt{\tilde{h}\left(\tilde{h}^3\frac{\rho^6}{r_H^6}\cos^6\theta - 8\tilde{d}^2\right)}}. \quad (4.19)$$

For solutions that reach the horizon of the black hole (i.e. which wrap the cigar D_2), we deduce from the above expression that

$$|\tilde{d}| \leq \cos^3\theta\big|_{\rho=r_H}. \quad (4.20)$$

The explicit relation between the density $\tilde{d}$ and the chemical potential μ_I follows from integrating eq. (4.19)

$$\alpha - \frac{\mu_I}{T} = \sqrt{\lambda}\,\tilde{d}\int_1^\infty dy \frac{(1-y^{-4})\sqrt{1+y^2\theta'(y)^2}}{\sqrt{(1+y^{-4})\left((1+y^{-4})^3 y^6\cos^6\theta - 8\tilde{d}^2\right)}}. \tag{4.21}$$

Here, the dimensionless variable $y = \rho/r_H$.

The D7-brane configurations that reach the horizon are referred to as "black hole embeddings". Analysis of the spectral functions of various fluctuations around such solutions reveals a continuous, gapless spectrum [59, 60] leading to the interpretation that these describe a phase where the "mesonic" fluctuations have melted in the high temperature plasma.

4.4.1 The action

Evaluated on the solution for $B + 2\pi\alpha' F$, the unrenormalized D7-brane action is

$$S_{D7} = \lambda N_f N \frac{T^3}{64}\int d^3x \int_1^\infty dy\, y^6 (1-y^{-4})(1+y^{-4})^{5/2} \frac{\cos^6\theta\sqrt{1+y^2\theta'(y)^2}}{\sqrt{(1+y^{-4})^3 y^6\cos^6\theta - 8\tilde{d}^2}}. \tag{4.22}$$

Note that this action cannot be varied to obtain the correct equations of motion for $\theta(y)$. The equation of motion for θ follows as usual by varying (4.15) or by using a different action where we trade A_τ for $F_{\tau\rho}$ as the independent variable, the equation for the latter being algebraic. This is achieved by the Legendre transform,

$$S_{D7} \to S_{D7}^{\rm LT} = S_{D7} - d\int \beta\, d^3x \int d\rho \left(F_{\tau\rho} + \frac{B_{\tau\rho}}{2\pi\alpha'}\right). \tag{4.23}$$

The resulting Legendre transformed action can be evaluated on the solution for F, to yield

$$S_{D7}^{\rm LT} = \lambda N_f N \frac{T^3}{64}\int d^3x \int_1^\infty dy\, y^3\, h\tilde{h}\sqrt{1+y^2\theta'(y)^2}\left(1 - \frac{8\,\tilde{d}^2}{\tilde{h}^3\, y^6\,\cos^6\theta}\right)^{1/2}\cos^3\theta\,. \tag{4.24}$$

It is easily verified that the corresponding expressions for real densities and real chemical potential can be obtained by the replacement $\tilde{d} \to i\tilde{d}$.

4.4.2 $m_q = 0$: constant solutions

It is straightforward to see that the DBI action admits constant solutions with $\theta = 0$ for a range of densities $\tilde{d}$. Since the constant solutions extend all the way to the horizon, they describe a phase of melted mesons. They also correspond to having vanishing masses for the fundamental hypermultiplets. In general, the large ρ asymptotics of $\theta(\rho)$ can be easily seen to be

$$\theta(\rho) = \frac{\theta_{(0)}}{\rho} + \frac{\theta_{(2)}}{\rho^3} + \dots, \tag{4.25}$$

where the coefficients $\theta_{(0)}$ and $\theta_{(2)}$ are related to the quark mass and condensate respectively. According to the AdS/CFT dictionary, this boundary behaviour signals the fact

JHEP07(2010)056

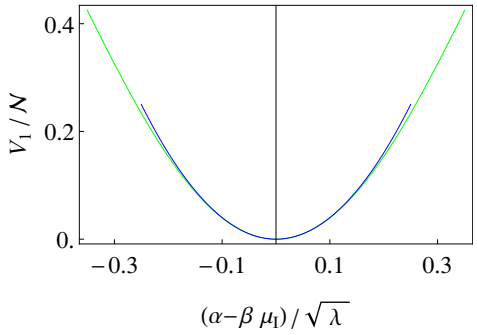

Figure 3. The potential for α from the flavours, as a function of $(\alpha - \mu_I/T)/\sqrt{\lambda}$. The curve in green is the full potential implied by the DBI action. The curve in blue is the quadratic piece that is consistent to keep in the $\lambda \to \infty$ limit. The normalization constant $\mathcal{N} = N_f N T^3 \lambda/16$.

that θ is dual to a dimenson 3 operator, namely, the quark bilinear. From the earlier description of the D3-D7 system and from eq. (4.6), the asymptotic value of $\rho \sin\theta$ is the D3-D7 separation, which is the quark mass i.e., $\theta_{(0)} = 2\pi\alpha' m_q$. The coefficient of the subleading term, namely $\theta_{(2)}$, determines the VEV of the same operator, *i.e* the quark condensate $\langle \Sigma_m \rangle = \langle \tilde{\psi}_i \psi_i \rangle + \ldots$.

It follows then that the solution with $\theta = 0$ has $m_q = 0$, $\langle \tilde{\Sigma}_m \rangle = 0$. When the slipping angle θ is vanishing, the D7-brane wraps the equatorial S^3 inside the five-sphere in the geometry. For this solution, the contribution of the flavours to the effective potential for α can be computed analytically.[4] From eq. (4.21) we find

$$\frac{1}{\sqrt{\lambda}}\left(\alpha - \frac{\mu_I}{T}\right) = \frac{\tilde{d}}{2}\int_1^\infty d\hat{y}\frac{1}{\sqrt{\hat{y}^6 - \tilde{d}^2}} = \frac{\tilde{d}}{12}\,|\tilde{d}|^{-2/3}\,B_{\tilde{d}^2}\left(\frac{1}{3},\frac{1}{2}\right), \tag{4.26}$$

where $B_z(a,b)$ is the incomplete beta function and the integration variable $\hat{y}$ is related to y as $\hat{y}^2 = \frac{1}{2}(y^2 + y^{-2})$. The action is formally divergent and requires renormalizaton which is achieved by a simple subtraction for the constant solutions,

$$\begin{aligned} S_{D7}^{\rm ren} &= \lambda N_f N \frac{T^3}{16}\int d^3x \int_1^\infty d\hat{y}\left(\frac{\hat{y}^6}{\sqrt{\hat{y}^6 - d^2}} - \hat{y}^3\right) \\ &= \lambda N_f N \frac{T^3}{96}\int d^3x \left[|\tilde{d}|^{4/3}\,B_{\tilde{d}^2}\left(-\frac{2}{3},\frac{1}{2}\right) + \frac{3}{2}\right]. \end{aligned} \tag{4.27}$$

The effective potential induced by the flavours can be found by eliminating $\tilde{d}$ from equations (4.26) and (4.27). It is important to note that since α is a phase defined modulo 2π, and likewise, the imaginary chemical potential μ_I is also a periodic variable, the combination $\alpha - \mu_I/T$ is bounded.

In the strong coupling limit $\lambda \gg 1$, we must therefore have that

$$\tilde{d} = \frac{4}{\sqrt{\lambda}}(\alpha - \mu_I/T) + \mathcal{O}(1/\lambda), \tag{4.28}$$

[4]The same expressions were obtained in [26] for the zero mass 'black hole embedding' solutions for real baryonic chemical potential.

JHEP07(2010)056

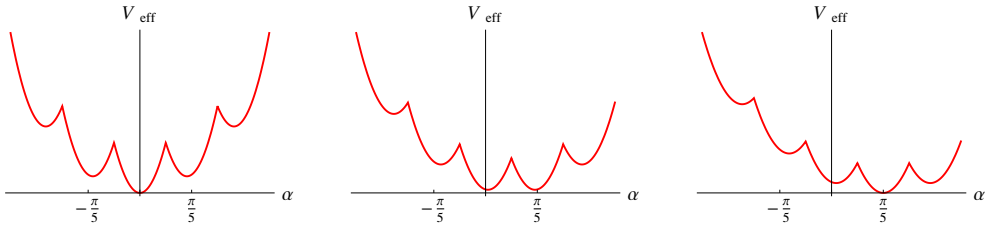

Figure 4. The full effective potential as a function of α from the flavours for three different values of μ_I/T. As μ_I/T is increased from left to right, the local minima of the effective potential compete, resulting in a first order phase transition.

by inverting eq. (4.26). Since $|\tilde{d}| \ll 1$ at strong coupling, we can expand the action (4.27) for small $\tilde{d}$ to obtain the contribution to the effective potential from the flavours,

$$V_f = N_f N T^4 \left(\alpha - \frac{\mu_I}{T}\right)^2 + \mathcal{O}(1/\sqrt{\lambda}). \qquad \alpha, \frac{\mu_I}{T} \in [-\pi, \pi], \tag{4.29}$$

which is independent of λ at the leading order in the strong coupling limit. The full effective potential at strong 't Hooft coupling with $N_f \ll N$ in the deconfined phase is then

$$V_{\text{eff}} = V_A + V_f = \min_{r\in\mathbb{Z}} 4\pi^2 N^2 \frac{T^4}{\lambda}\left(\alpha - \frac{2\pi r}{N}\right)^2 + N_f N T^4 \left(\alpha - \frac{\mu_I}{T}\right)^2. \tag{4.30}$$

From this effective potential it is obvious that the degeneracy of the $\mathbb{Z}_N$ vacua has been lifted by the massless fundamental flavour fields. Curiously, while the flavour contribution is $\mathcal{O}(1/N)$ suppressed compared to the leading term in the large N limit, it is unsuppressed by powers of the 't Hooft coupling λ in the strong coupling limit. The order of limits is, of course, unambiguous in the present context since N is taken to infinity first, keeping the 't Hooft coupling fixed and large.

There are N local minima, but a unique global minimum at $\alpha = 0$ when $\mu_I = 0$. As μ_I is increased smoothly from zero and approaches $\mu_I = \pi/N$, two neighboring minima become degenerate and any further increase in μ_I results in a first order phase transition from the $\alpha = 0$ vacuum to the vacuum with $\alpha = 2\pi/N$ (see figure (4)).

Free energy: as the phase transitions at $\mu_I/T = (2r-1)\frac{\pi}{N}$ for $r \in \mathbb{Z}$ are first order, it is useful to compute the free energy as a function of the imaginary chemical potential μ_I. The free energy (the grand potential) density can be calculated by minimizing the effective potential eq. (4.30) with respect to α for all μ_I and we find

$$\begin{aligned} F[\mu_I]\Big|_{\lambda\gg 1} &= N_f N T^4 \left(1 + \frac{\lambda}{4\pi^2}\frac{N_f}{N}\right)^{-1} \min_{r\in\mathbb{Z}} \left(\frac{\mu_I}{T} - \frac{2\pi r}{N}\right)^2, \\ &\simeq N_f N T^4 \min_{r\in\mathbb{Z}} \left(\frac{\mu_I}{T} - \frac{2\pi r}{N}\right)^2. \end{aligned} \tag{4.31}$$

While the quadratic behaviour is simply a consequence of large N, it is interesting to compare the coefficient with the result at weak coupling and zero hypermultiplet mass

eq. (2.6). Since we have $2N_f$ complex scalars and $2N_f$ Weyl fermions, the free energy at weak coupling (and $m_q = 0$) is

$$F[\mu_I]\Big|_{\lambda\ll 1} = \frac{1}{2}\, NN_f T^4 \min_{r\in\mathbb{Z}} \left(\frac{\mu_I}{T} - \frac{2\pi r}{N}\right)^2 . \tag{4.32}$$

We observe that the strong and weak coupling results differ by a factor of 2.

4.4.3 $m_q \neq 0$ non-constant solutions

Solutions with non-zero quark mass also happen to be non-constant and these need to be understood numerically. For smooth solutions that get to the horizon from the boundary, we require that the $S^3 \subset S^5$ wrapped by the D7-brane remains non-vanishing along the solution. As is well-known, there are two classes of non-constant D7-brane solutions: those that get all the way to the horizon (the so-called "black-hole embeddings"), and those that end smoothly before they get to the horizon. For both classes of solutions, the quark mass and the condensate can be read off from the asymptotic behaviour (4.25) near the boundary of AdS_5. Specifically, in terms of the dimensionless variable $y = \rho/r_H$, the boundary behaviour of the slipping angle is

$$\theta(y) = \frac{2}{\sqrt{\lambda}} \left(\frac{m_q}{T}\right) \frac{1}{y} + \frac{\theta_{(2)}}{\pi^3 T^3 R^6} \frac{1}{y^3} + \dots . \tag{4.33}$$

Note that it is only the ratio m_q/T which is relevant here, since the theory without hypermultiplets is the conformal $\mathcal{N} = 4$ theory without an intrinsic scale. We thus define the natural dimensionless ratio that characterizes these solutions,

$$\frac{M}{T} \equiv \frac{2m_q}{\sqrt{\lambda}T}, \tag{4.34}$$

where the mass scale $M = 2m_q/\sqrt{\lambda}$ is the characteristic scale of meson bound states at zero temperature (and strong coupling) [31].

The Euclidean action for these solutions requires careful renormalization via subtractions to yield finite results. The correct procedure of holographic renormalization has been developed for probe Dp-branes in AdS spacetime [32, 54]. The result of this procedure in the present context is that the renormalized action is defined as an integral over y from $y = 1$ (the IR) to $y = \Lambda$ (a UV cutoff) along with counterterms defined locally at $y = \Lambda$,

$$S_{D7}^{\text{ren}} = S_{D7}\big|_{\Lambda} - \lambda N_f N \frac{T^3}{64} \left(\frac{1}{4}\Lambda^4 - \frac{1}{2}\Lambda^4\theta(\Lambda)^2 + \frac{5}{12}\Lambda^4\theta(\Lambda)^4\right). \tag{4.35}$$

The first two counterterms are divergent while the third is a finite subtraction. Further counterterms are necessary if the boundary is not flat.

Black-hole embeddings: solutions extending all the way to the black hole horizon, often referred to as "black-hole embeddings" of the D7-brane, satisfy $\theta'(y = 1) = 0$ and $0 \leq \theta(y = 1) < \frac{\pi}{2}$. Thus for these embeddings, the S^3 remains blown-up all along the solution, while the S^1 (the thermal circle) shrinks at the horizon, so the D7-brane caps off

JHEP07(2010)056

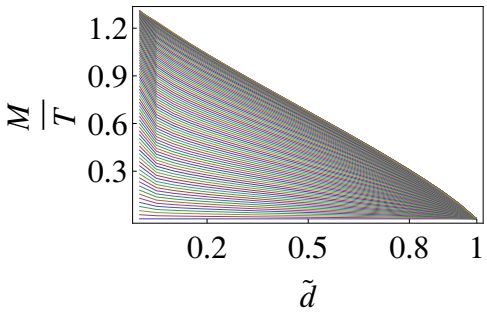

Figure 5. The values of $\frac{M}{T}$ and the density variable $\tilde{d}$ (conjugate to imaginary μ) for which the black hole embeddings or melted meson solutions exist.

smoothly. By varying $\theta(y=1)$ we can explore different values of the hypermultiplet mass M/T. These Euclidean solutions can exist only if

$$|\tilde{d}| \leq \cos^3\theta\big|_{y=1}. \tag{4.36}$$

The black hole embeddings describe a high temperature phase where mesons have melted.

For a fixed density $\tilde{d}$, solutions with different hypermultiplet masses can be found by dialling $\theta(y=1)$ provided the condition (4.36) is satisfied. As in the massless case analyzed above, we will obtain (numerically) the effective potential as a function of $(\alpha - \mu_I/T)/\sqrt{\lambda}$. We summarize the properties of the solutions below.

- The solutions for finite density $0 < |\tilde{d}| \leq 1$, are all of the type described above and are qualitatively similar to black-hole embeddings found earlier for vanishing baryonic chemical potential [16, 19]. They are qualitatively distinct from the configurations with real chemical potential [22, 23, 26, 27]. We elaborate on this below.

- For any given density $|\tilde{d}|$ (between 0 and 1) there is a fixed value of M/T, above which solutions cease to exist. The allowed range of masses decreases with increasing $|\tilde{d}|$ (figure 5). When the density $\tilde{d}$ approaches unity, all allowed solutions bunch up near the zero mass constant solution. This is illustrated in figure 6 where we plot solutions in the $\rho_1 - \rho_2$ plane ($\rho_2 = \rho\sin\theta$ and $\rho_1 = \rho\cos\theta$). In contrast to this picture, for a real chemical potential, it was observed (e.g. in [22, 26]) that black hole embeddings can exist at all possible values of the ratio M/T. For large values of the mass (or low temperatures), these solutions could be viewed as a probe D7-brane with strings (quarks) attached which drop into the black hole horizon. The absence of these kinds of solutions substantially alters the phase diagram for imaginary chemical potential.

- The largest value of the ratio $\frac{M}{T} = \frac{2m_q}{\sqrt{\lambda}T}$ for which the black hole embedding exists is ≈ 1.30 and this occurs when $\tilde{d} = 0$ and is the critical embedding solution (figure 10).

- By evaluating the action and the expectation value of the quark condensate operator $\langle\Sigma_m\rangle$, for a given density $\tilde{d}$, we may see that for large enough masses, there exist two classical solutions with the same mass but different values for the action and

JHEP07(2010)056

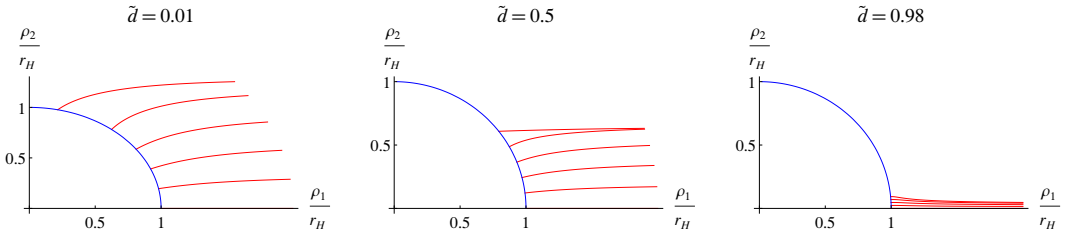

Figure 6. D7-brane solutions extending to the horizon for $\tilde{d} = 0.01$, 0.5 and 0.98. For each density we have plotted a family of solutions with increasing masses up to the maximum value allowed for that density. The asymptotic distance from the ρ_1 axis gives the ratio M/T. The black hole horizon is the blue curve $\rho_1^2 + \rho_2^2 = r_H^2$.

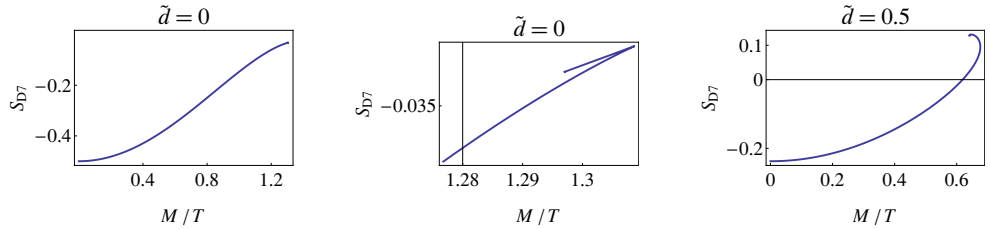

Figure 7. The action as a function of M/T for $\tilde{d} = 0$ and $\tilde{d} = 0.5$.

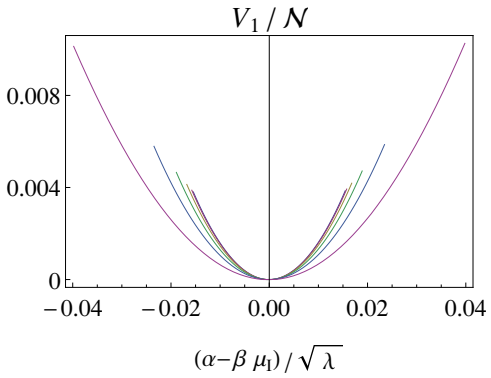

Figure 8. The effective potential from flavours for increasing values of m_q, for $M/T = 0$, 0.24, 0.48, 0.72, 0.96 and 1.2. The potential tends to flatten out as M/T approaches the critical value of 1.3.

condensate (figure 7). This feature, well-known at zero density, also appears for non-zero densities conjugate to an imaginary chemical potential. The solution with the lower action is then chosen to be the physical one.

The effective potential: the contribution to the effective potential for the phase of the Polyakov-Maldacena loop α, can be found numerically (figure 8). However, we can already be fairly precise about the form of this contribution due to eq. (4.21): since α and μ_I/T are bounded, we must have that $|\tilde{d}| \sim \mathcal{O}(1/\sqrt{\lambda}) \ll 1$. Notice that this scaling of $\tilde{d}$, actually implies that the dimensionful density $d \sim N_f N T^3$, which is a natural scaling for N_f quark flavors. In taking $\tilde{d} \sim \mathcal{O}(1/\sqrt{\lambda})$, we are also assuming that the integral in eq. (4.21) is well-

JHEP07(2010)056

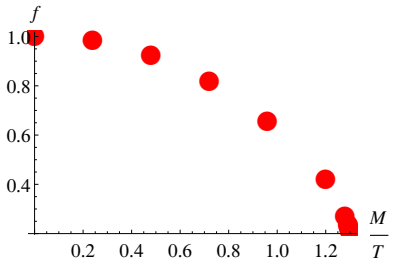

Figure 9. The dimensionless coefficient f in the quadratic effective potential V_f due to hypermultipltes.

behaved as $\tilde{d} \to 0$ and we can check numerically that this is the case for all hypermultiplet masses in the range $0 \leq \frac{M}{T} \lesssim 1.30$ corresponding to the black hole embedding solutions. In addition since the D7-brane action is a function of $\tilde{d}^2$, for small $\tilde{d}$, it can be expanded in powers of $\tilde{d}^2$. In the large λ limit, the quadratic piece alone dominates and therefore we find that the effective potential is of the form

$$V_{\text{eff}} = V_A + V_f = \min_{r\in\mathbb{Z}} 4\pi^2 N^2 \frac{T^4}{\lambda}\left(\alpha - \frac{2\pi r}{N}\right)^2 + N_f N T^4 f\left(\frac{M}{T}\right)\left(\alpha - \frac{\mu_I}{T}\right)^2 . \quad (4.37)$$

Here M is the mass scale $\frac{2m_q}{\sqrt{\lambda}}$ and f is a dimensionless function of $\frac{M}{T}$. The coefficient $f\left(\frac{M}{T}\right)$ is unity when $m_q = 0$ and decreases monotonically with increasing mass, eventually approaching ≈ 0.2 as $\frac{M}{T}$ is dialled to its maximum value of approximately 1.3 (figure 9). We should emphasize that in deriving the effective potential above, in the large λ and large N limit, we only needed to use solutions with small $\tilde{d}$, strictly only those in the vicinity of $\tilde{d} \sim \mathcal{O}(1/\sqrt{\lambda})$. When we turn to the low temperature regime below, we will see that this is actually crucial for ensuring a consistent picture of the transition between high and low temperatures.

To summarize, for all values of the parameter $\frac{M}{T}$ for which black hole embeddings of the D7-brane exist, with an imaginary chemical potential, first order Roberge-Weiss transitions will occur at $\frac{\mu_I}{T} = (2r-1)\frac{\pi}{N}$, $r \in \mathbb{Z}$. This means that, for fixed hypermultiplet mass m_q, the RW transition will occur for temperatures $T \gtrsim 2m_q/(1.3\sqrt{\lambda})$. We will determine the value of this temperature, representing the RW endpoint, more precisely below.

The monotonic decrease in $f(M/T)$ with decreasing temperature (or increasing mass m_q) is in accord with intuition from weak coupling. The quadratic potential for α can be interpreted as a thermal contribution to the mass of the mode α from the flavours. That this thermal correction should decrease as the flavours are made heavier (eventually decoupling for infinite mass), appears intuitively to be consistent. At weak coupling, it would be natural to identify the mass of the mode α with the Debye mass (inverse electric screening length). It is unclear whether any such interpretation should be possible at strong coupling. Finally, we can again write the free energy as a function of μ_I, (taking $\lambda N_f/N \ll 1$),

$$F[\mu_I] = N_f N T^4 f\left(\frac{m_q}{2\sqrt{\lambda}T}\right) \min_{r\in\mathbb{Z}} (\alpha - \mu_I/T)^2 . \quad (4.38)$$

JHEP07(2010)056

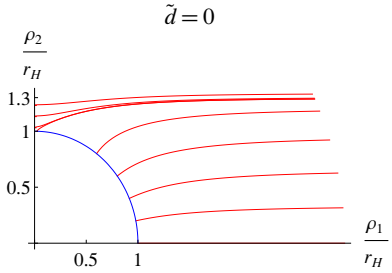

Figure 10. The well known transition at zero density, from black hole embeddings (falling into the black hole) to Minkowski embedding probe D7-branes placed away from the horizon.

Given our numerical results for f, we can say that near $m_q = 0$, $f \approx 1 - f''(0)\frac{m_q^2}{8\lambda T^2}$. In contrast, in the weakly coupled theory the coefficient in eq. (2.6) (with $n_f = \tilde{n}_f = 2N_f$) decreases *linearly* with mass, for small enough mass, and is independent of the weak 't Hooft coupling at leading order

$$\frac{1}{6}\left(\, f_{\rm bose}(m_q/T) + f_{\rm fermi}(m_q/T)\,\right) \approx \frac{1}{2} - \frac{|m_q|}{T}\,\frac{\pi}{18} + \dots \tag{4.39}$$

The origin of the linear term can be traced to the pole in the Bose-Einstein distribution for free massless bosons at zero momentum. The absence of a linear term at strong coupling is perhaps indicative of the strong dressing undergone by the perturbative scalar degrees of freedom. It is also worth noting that at strong coupling, the natural dimensionful parameter is the meson mass scale M, rather than the hypermultiplet quark mass m_q.

Low temperatures/large masses, $M \gtrsim 1.3$: the critical black hole embedding of the D7-brane has the property that the slipping angle θ of the solution approaches $\frac{\pi}{2}$ at the horizon and the corresponding S^3 wrapped by the probe brane shrinks. Hence, the only solutions with masses higher than $\frac{M}{T} \approx 1.3$ are those where the S^3 wrapped by the D7-brane shrinks before the D7-brane gets to the horizon. For these embeddings the thermal S^1 remains non-vanishing while the S^3 shrinks smoothly before the brane gets to the horizon. Since the S^3 shrinks at the tip of such a solution, we are forced to have $\tilde{d} = 0$ due to eq. (4.36) and hence

$$F_{\tau\rho} + 2\pi\alpha' B_{\tau\rho} = 0. \tag{4.40}$$

The D7-brane action has no dependence on either α or μ_I. Hence there is no potential induced by flavours for the phase α of the Polyakov-Maldacena loop: $V_f(\alpha - \mu_I/T)$ vanishes identically and the physics is completely smooth as a function μ_I. Note that despite the fact that the field strength F is fixed by B, we can always add a constant to the world-volume gauge potential A_τ, which will not change the field strength, and can be interpreted as a chemical potential μ_I in the boundary field theory. Hence, in the grand canonical ensemble, at low temperatures ($T \ll M$), for every μ_I the only solution possible is the $\tilde{d} = 0$ Minkowski embedding representing unmelted mesons. The situation is quite distinct from the case of real chemical potential [27] wherein, at fixed low temperatures, there is a

JHEP07(2010)056

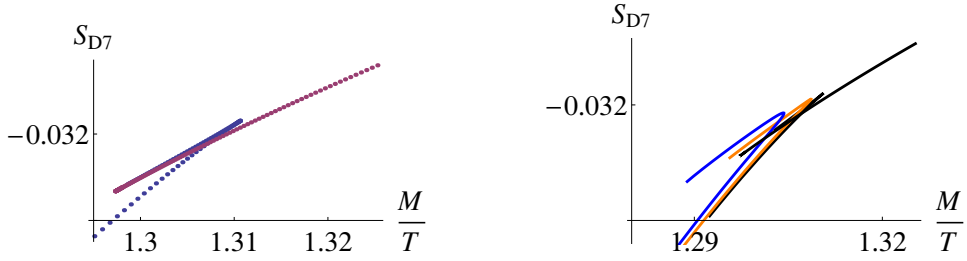

Figure 11. *Left*: The action for $\tilde{d} = 0$, D7-brane embeddings. As the ratio M/T is increased, just before the black hole embedding (melted meson) ceases to exist, there is a transition to the family of so-called "Minkowski embeddings" corresponding to unmelted mesons. *Right:* In the second figure we see that the action (grand potential) for black hole embeddings with $\tilde{d} > 0$, (0.004 (orange) and 0.008 (blue)), is always larger than the action for the $\tilde{d} = 0$ solutions (black). There is no Minkowski embedding solution with $\tilde{d} \neq 0$.

transition from Minkowski embedding solutions to the spiky black hole embeddings as the chemical potential is increased.

The solutions with $\tilde{d} = 0$ are the same as those originally obtained in [16, 19, 21]. The transition from the black hole embeddings to the second class of solutions involves a topology change: the first category of solutions exhibits a shrinking S^1 and a finite S^3, while the second has the S^3 shrinking in the interior. The transition between these is well-known and is a first order phase transition as may be inferred from plotting the action as a function of M/T (figure 11) for the solution with $\tilde{d} = 0$. The phase transition between the two classes of solutions is a "meson-melting" transition. At low enough temperatures (or large enough hypermultiplet mass), the only allowed D7-brane embeddings are the unmelted mesons with zero density $\tilde{d} = 0$. The spectrum of fluctuations about this solution exhibits a mass gap and a discrete spectrum [31] at zero temperature. The mass gap in the meson spectrum is

$$M_{\rm gap} = 4\pi \frac{m_q}{\sqrt{\lambda}} = 2\pi M. \tag{4.41}$$

We also see that as the density $\tilde{d}$ is increased from zero, for small enough densities $\tilde{d} \ll 1$, the black hole embeddings with $\tilde{d} \neq 0$ coexist with the zero density $\tilde{d} = 0$ Minkowski embedding solution for a range of temperatures (figure 11). This will be important for determining the phase diagram and the shape of the phase boundaries in the grand canonical ensemble. With increasing density, there is a critical value of $\tilde{d}$, ($\gtrsim 10^{-2}$) beyond which the curves for black hole embeddings (as in figure 11) cease to intersect the Minkowski solution at $\tilde{d} = 0$. They turn back and terminate at progressively smaller values of M/T (figure 7). The presence of such configurations in the grand canonical ensemble could make the low temperature region of the phase diagram inaccessible. However, it should be clear from the preceding discussions that these configurations are essentially removed as a consequence of the Roberge-Weiss transition. The RW transitions occur at values of $(\alpha - \mu_I/T)$ that are parametrically suppressed by $1/N$ corresponding to parametrically small values of $\tilde{d}$. The configurations with such low densities will always be of the kind depicted in figure 11.

JHEP07(2010)056

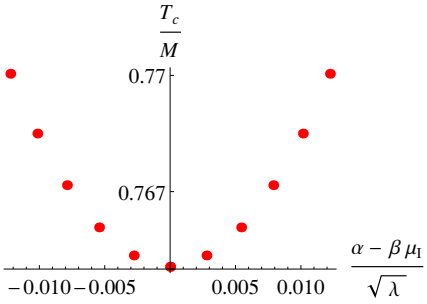

Figure 12. The melting transition temperature at different values of μ_I and fixed α.

5 Phase diagram

The above analysis of the dominant configurations at different densities and temperatures now allows us to determine the phase diagram of the theory as a function of the temperature/meson mass scale ratio T/M and the imaginary chemical potential μ_I. We have already established that at low temperature the physics is independent of μ_I and α, the phase of the Polyakov loop, and is dominated by the unmelted meson (Minkowski embeddings) configurations with vanishing density $\tilde{d} = 0$. In addition, we have seen that at high temperature the dominant configurations are the black hole embeddings representing melted mesons with $\tilde{d} \neq 0$. For these configurations the system experiences a first order phase transition at $\mu_I/T = (2r-1)\pi/N$ $(r \in \mathbb{Z})$, characterized by a discrete jump in the phase of the Polyakov loop. Specifically, α jumps from $2\pi(r-1)/N$ to $2\pi r/N$.

What remains is to understand the phase boundary between the melted and unmelted meson phases as a function of μ_I. We first recall that in the melted phase $\tilde{d}$ is proportional to $(\mu_I/T - \alpha)/\sqrt{\lambda}$, for small enough $\tilde{d}$. As depicted in figure 11, in the grand canonical ensemble, the melted meson configuration with small $\tilde{d} \neq 0$ will then have to compete with the $\tilde{d} = 0$ Minkowski embedding as the temperature is decreased. This results in a first order transition between the two phases. It is clear from figure 11 that as the density increases (for positive $\tilde{d}$, say), the transition temperature increases as well (equivalently M/T decreases). The dependence of this transition temperature on the chemical potential determines the shape of the phase boundary in the $\mu_I - T$ plane. We can numerically obtain the melting transition temperatures $T_c(\mu_I)$ for different values of μ_I (corresponding to different densities $\tilde{d}$ in the melted phase). The result is shown in figure 12. For

$$\alpha = \frac{2\pi r}{N}\,, \qquad (2r-1)\frac{\pi}{N} \leq \frac{\mu_I}{T} < (2r+1)\frac{\pi}{N}\,, \qquad r \in \mathbb{Z}, \tag{5.1}$$

we find that

$$T_c(\mu_I) - T_0 = K\,\frac{M}{\lambda}\left(\frac{\mu_I}{T_c(\mu_I)} - \alpha\right)^2 + \ldots\,, \qquad K \approx 33.5$$

where $T_0 = T_c(0) \approx 0.77M$. We have only kept terms to quadratic order on the right hand side for two reasons: First, since the difference $\mu_I/T - \alpha$ is bounded, higher order terms

JHEP07(2010)056

are suppressed at strong coupling ($\lambda \gg 1$). Secondly, we also have that $|\mu_I/T - \alpha| \leq \pi/N$, so higher order terms are suppressed by powers of $1/N^2$. At leading order in $1/\lambda$, $T_c(\mu_I)$ may therefore be replaced by T_0 on the right-hand side of (5.2).

The first-order phase boundary between the melted phase at high temperature and the unmelted phase at low temperature has the curvature as shown in figure 1. Combining this result with the Roberge-Weiss lines at $\mu_I = \mu_{\rm RW}$ yields an infinite set of points at which three first order transition lines meet. At each of these *triple points*, three phases labelled by distinct values of the Polyakov loop coexist. The location of the triple points in the $\mu_I - T$ plane is given by $(\mu_{\rm RW}, T_{\rm RW})$, where

$$\frac{\mu_{\rm RW}}{T_0} = (2r-1)\frac{\pi}{N}, \qquad \frac{T_{\rm RW}}{T_0} = 1 + \frac{\kappa}{\lambda}\frac{\pi^2}{N^2}, \tag{5.2}$$

with $r \in \mathbb{Z}$ and $\kappa = KM/T \approx 43.5$. The N-scaling of the formulae may suggest that these should be subleading effects in the large-N limit and therefore not consistently incorporated in a classical supergravity approximation. However the factors of $1/N$ arise from purely kinematical considerations, namely the symmetry of the theory under shifts $\mu_I \to \mu_I + 2\pi/N$. When N is large, the RW transitions are closely spaced, resulting in the N-dependence in the Roberge-Weiss temperature. The curvature of the phase boundary in figure 1 is independent of N, see eq. (1.2).

5.1 Real chemical potential and analytical continuation

For real values of the quark density a rich family of solutions to the DBI equations of motion exists, after making the replacement $F \to iF$ (and setting $B = 0$) in eq. (4.15). In particular, black hole embeddings, representing melted mesons, exist for all values of the ratio M/T in the canonical ensemble with fixed quark number density. These include low temperature ($M \gg T$) solutions which can be viewed as Minkowski embeddings attached to a spike consisting of strings (quarks) falling into the black hole horizon.

The phase diagram for real chemical potential in the grand canonical ensemble [23, 25–27] bears little relation to figure 1, either at low or high temperatures. With a real quark chemical potential, there is a single line of phase transitions separating a zero density phase from the dissociated or melted meson phase. For small chemical potential the transition line is first order, while at larger chemical potential the transition is expected to be a continuous one [26, 61–63], terminating at $\mu = m_q$. In fact it has been argued in [61, 62] that for low temperatures the transition line is actually third order and connects up with the first order line at a tricritical point.

In the context of QCD, the main motivation behind the exploration of the phase diagram as a function of imaginary chemical potential has been to determine the phase structure for real chemical potential, via the use of analytic continuation from imaginary $\mu = i\mu_I$ (with $\mu^2 < 0$) to real μ (with $\mu^2 > 0$) [35–45]. It is therefore natural to ask what aspects of the phase diagram can be captured by analytic continuation in the holographic model we studied here. This is particularly interesting given the qualitative difference in the nature of black hole embeddings and the D7-brane solutions at fixed density. At large real or imaginary chemical potential the phase structures are manifestly different due to

JHEP07(2010)056

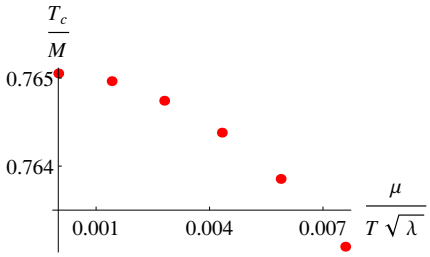

Figure 13. The line of first order meson-melting transitions for real chemical potential, $\mu \gtrsim 0$.

the presence of the Roberge-Weiss transitions. However it is expected that the curvature of the meson melting line for imaginary chemical potential, with $\mu^2 < 0$, is directly related to the curvature of the first order transition line for real chemical potential, with $\mu^2 > 0$. Repeating the analysis for real chemical potential we find that the curvature of the first order line for $\mu^2 > 0$ is given by (see figure 13)

$$T_c(\mu) - T_0 \approx -33.5 \, \frac{M}{\lambda} \frac{\mu^2}{T_0^2}, \tag{5.3}$$

matching up with our result for imaginary μ. It is reassuring that despite the differences between individual D7-brane probe solutions for $\mu^2 \gtrless 0$, the theory is analytic in μ^2 near $\mu^2 = 0$.

6 Discussion

In the presence of an imaginary quark chemical potential μ_I the D3-D7 holographic setup at strong coupling displays a first-order meson melting transition at $T = T_c(\mu_I)$ and a set of first-order Roberge-Weiss transitions at fixed $\mu_I = \mu_{\rm RW}$ in the high-temperature phase $T > T_c(\mu_I)$. The first-order lines join at a series of triple points in the $\mu_I - T$ plane. We have determined the location of the triple points and the curvature of the phase boundaries, and confirmed that the theory is analytic in μ^2 near $\mu^2 = 0$.

Since the adjoint degrees of freedom are always deconfined in this model, the quark (or meson) mass and the temperature cannot be varied independently in the absence of another scale. The model of Sakai and Sugimoto [15] would be more "QCD-like" in this context and it would therefore be interesting to compute the order of the thermal phase transition and the Roberge-Weiss endpoint in that model. Recently, it has been demonstrated in QCD that the Roberge-Weiss endpoints are triple points for two [43] or three [38] degenerate light or heavy flavours, and second order endpoints in the 3d Ising universality class for intermediate quark masses. It would be extremely interesting to find a holographic model where the triple points turn into second order endpoints, as the quark mass m_q is varied. This could be realized in models incorporating backreaction of flavours or in defect models in general Dp-Dq setups [63].

JHEP07(2010)056

Acknowledgments

We would like to acknowledge an STFC rolling grant for support. We thank Paolo Benincasa for comments on a draft version of this paper; Owe Philipsen and Massimo d'Elia for discussions.

A One-loop free energy at weak coupling

To calculate the perturbative contributions to the free energy at finite temperature, in the presence of an imaginary chemical potential, we need to first understand the perturbative effective potential for the Polyakov loop degrees of freedom. The computation is fairly standard, so we will only present a brief summary (we refer the reader to [9, 51, 52, 64] for details of the theory on flat space and on $S^3 \times \mathbb{R}$). At finite temperature, for the SU(N) gauge theory, we introduce the Wilson line around the thermal circle as

$$U = \exp i \left(\int_0^\beta A_\tau \, d\tau \right) . \tag{A.1}$$

Picking a gauge where the zero mode of A_τ is diagonal

$$\mathcal{A} \equiv \int_0^\beta A_\tau \, d\tau \; = \; \mathrm{Diag}(\alpha_1, \alpha_2, \ldots \alpha_N), \qquad \sum_{i=1}^{N} \alpha_i = 0 \bmod 2\pi, \tag{A.2}$$

we want to compute the perturbative contributions to the thermal partition function in the presence of these VEVs. Let us suppose that the SU(N) gauge fields are coupled to $\tilde{n}_A$ adjoint Weyl fermions and n_A real scalars also in the adjoint representation of the gauge group. In addition we allow for $\tilde{n}_f$ Weyl fermions and n_f complex scalars all in the fundamental representation of SU(N). The one-loop result for the effective action then has the general form

$$\begin{aligned} S_{1-\mathrm{loop}} \; & \frac{1}{2} \log\det \left(-\mathcal{D}_0^2 - \nabla^{2(v)} \right) + \frac{n_A}{2} \log\det \left(-\mathcal{D}_0^2 - \nabla^2 \right) \\ & + n_f \, \log\det \left(-\tilde{D}_0^2 - \nabla^2 + m^2 \right) - \tilde{n}_A \log\det \left(i\gamma^0 \mathcal{D}_0 + i\gamma^i \partial_i \right) \\ & - \tilde{n}_f \log\det \left(i\gamma^0 \tilde{D}_0 + i\gamma^i \partial_i - m_q \right) . \end{aligned} \tag{A.3}$$

Here, we have allowed for a common mass m_q for the fields in the fundamental (f) representation in view of the fact that the theory that we investigate at strong coupling also falls in this class. The background field gauge covariant derivatives are defined as

$$\mathcal{D}_0 \equiv \partial_\tau + iT \, [\mathcal{A}, \,] \, , \qquad \tilde{D}_0 \equiv \partial_\tau + iT\mathcal{A} \, , \tag{A.4}$$

JHEP07(2010)056

when acting on adjoint and fundamental fields respectively. This one-loop effective action is then given by

$$S_{1-\text{loop}}/\text{Vol} \tag{A.5}$$
$$= \int_0^\infty \frac{dk}{2\pi^2}\, k^2 \left[\sum_{ij=1}^{N} \Big((2+n_A)\,\text{Re ln}\left(1 - e^{-i\alpha_{ij}}\, e^{-\beta k}\right) - 2\tilde{n}_A\,\text{Re ln}\left(1 + e^{-i\alpha_{ij}}\, e^{-\beta k}\right)\Big) \right.$$
$$\left. + \sum_{i=1}^{N} \left(2n_f\,\text{Re ln}\left(1 - e^{-i\alpha_i}\, e^{-\beta\omega_k}\right) - 2\tilde{n}_f\,\text{Re ln}\left(1 + e^{-i\alpha_i}\, e^{-\beta\omega_k}\right)\right)\right].$$

Here

$$\alpha_{ij} \equiv \alpha_i - \alpha_j\ , \qquad \omega_k \equiv \sqrt{k^2 + m_q^2}. \tag{A.6}$$

To evaluate the free energy as a function of the imaginary quark number chemical potential, we will consider the massless and massive cases separately, as the former can be studied exactly at the one-loop order.

Massless fundamental flavours: with $m = 0$ the integrals in eq. (A.5) can be done to yield the effective potential for the Polyakov loop variables (assuming $0 \le \alpha_i < 2\pi$ and $\sum \alpha_i = 0 \bmod 2\pi$),

$$V_{\text{eff}}\, \frac{\pi^2}{48} T^4 \left[\sum_{ij=1}^{N} \left\{ (2+n_A) \left(1 - \left(\frac{\alpha_{ij}}{\pi}\Big|_{\text{mod}\,2} - 1\right)^2\right)^2 \right.\right. \tag{A.7}$$
$$\left. - 2\tilde{n}_A \left(1 - \left(\left(\frac{\alpha_{ij}}{\pi} + 1\right)\Big|_{\text{mod}\,2} - 1\right)^2\right)^2 \right\}$$
$$\left. + \sum_{i=1}^{N} \left\{ 2n_f \left(1 - \left(\frac{\alpha_i}{\pi}\Big|_{\text{mod}\,2} - 1\right)^2\right)^2 - 2\tilde{n}_f \left(1 - \left(\left(\frac{\alpha_i}{\pi} + 1\right)\Big|_{\text{mod}\,2} - 1\right)^2\right)^2 \right\} \right].$$

It is easy to see that $\alpha_i = 2\pi k/N$, $k = 0, 1, 2, \ldots N-1$ are extrema of the action. The contributions from the adjoint degrees of freedom are naturally invariant under $\mathbb{Z}_N$ shifts $\alpha_i \to \alpha_i + 2\pi k/N$, while the fundamental flavours break the discrete symmetry. Expanding around each of the N extrema, we can show that they are each local *minima* labelled by the integer k, provided

$$N(2 + n_A + \tilde{n}_A) + \tilde{n}_f \left(1 - 12\frac{k^2}{N^2}\right) + 2n_f \left(1 - \frac{6k}{N} + \frac{6k^2}{N^2}\right) > 0. \tag{A.8}$$

As long as this condition is satisfied, at the 1-loop level, all N extrema of the effective potential will be local minima. While it is interesting to ask what the fate of the effective potential is, when the above condition is not satisfied, in the theory that we are interested in (namely, $\mathcal{N} = 4$ SYM coupled to N_f, $\mathcal{N} = 2$ hypermultiplets) — $n_A = 6$, $\tilde{n}_A = 4$, $\tilde{n}_f = n_f = 2N_f$ and $N \gg N_f$ — the extrema will always be local minima.

The global minimum of the effective potential is at $\alpha_i = 0$.

The effect of the imaginary chemical potential for the fundamental flavours is easily captured. Let us, for the sake of simplicity, restrict attention to the case where the complex

JHEP07(2010)056

scalars and fermions in the fundamental represention, all have the same (imaginary) chemical potential. Then, an imaginary chemical potential is introduced by the replacement,

$$\tilde{D}_0 \to \partial_\tau + iT\mathcal{A} - i\mu_I \mathbf{1}. \tag{A.9}$$

Therefore, the effective potential for $\mu_I \neq 0$ is the same as (A.7) with $\alpha_i \to \alpha_i - \beta\mu_I$. For small non-zero $\beta\mu_I$, the global minimum continues to be at $\alpha_i = 0$. However, when $\beta\mu_I = 2\pi r/N$, $(r \in \mathbb{Z})$ the global minimum shifts to $\alpha_i = 2\pi r/N$. This is simply because the effective potential from the fundamental flavours depends on $\alpha_i - \beta\mu_I$, whilst the adjoint sector is independent of μ_I. One concludes that as $\beta\mu_I$ is increased from 0, past π/N, the global minimum jumps to $\alpha_i = 2\pi/N$ following a first order phase transition. The free energy of the theory as a function of μ_I can now be calculated. This is done by first evaluating the the effective potential at a given global minimum $\alpha_i = 0$,

$$\begin{aligned}\mathcal{F}(\beta\mu_I) &\equiv V_{\text{eff}}(\alpha_i = 0) \\ &= NT^4\frac{\pi^2}{24}\left[n_f\left(1-\left(-\frac{\beta\mu_I}{\pi}\Big|_{\text{mod }2}-1\right)^2\right)^2 - \tilde{n}_f\left(1-\left(\left(-\frac{\beta\mu_I}{\pi}+1\right)\Big|_{\text{mod }2}-1\right)^2\right)^2\right].\end{aligned} \tag{A.10}$$

This yields the correct free energy, but only in the range $-\frac{\pi}{N} < \beta\mu_I < \frac{\pi}{N}$. Outside this range, for instance when $\beta\mu_I > \frac{\pi}{N}$, the global minimum moves to $\alpha_i = 2\pi/N$ and the free energy is given by the function $\mathcal{F}(\beta\mu_I - 2\pi/N)$. The correct free energy as a function of μ_I is

$$F[\mu_I] = \min_{r\in\mathbb{Z}} \mathcal{F}\left(\beta\mu_I - \frac{2\pi r}{N}\right), \tag{A.11}$$

a function with cusps at $\beta\mu_I = (2r-1)\pi/N$, $r \in \mathbb{Z}$.

When N is large, only the behaviour of F near its local minima is important, i.e.,

$$F[\mu_I]\Big|_{N\gg 1} = (2n_f + \tilde{n}_f)\, N\frac{T^4}{12}\min_{r\in\mathbb{Z}}\left(\beta\mu_I - \frac{2\pi r}{N}\right)^2. \tag{A.12}$$

Massive fundamental flavours: when $m \neq 0$, the effective potential eq. (A.5) cannot be expressed in simple analytical form. Nevertheless, it has the same qualitative properties as the $m_q = 0$ potential in the presence of non-vanishing μ_I. Specifically, we can follow the reasoning above to deduce the free energy at large N,

$$F[\mu_I] = N\frac{T^4}{12}\left[n_f\, f_{\text{bose}}\left(\frac{m_q}{T}\right) + \tilde{n}_f\, f_{\text{fermi}}\left(\frac{m_q}{T}\right)\right]\min_{r\in\mathbb{Z}}\left(\beta\mu_I - \frac{2\pi r}{N}\right)^2, \tag{A.13}$$

where

$$f_{\text{bose}}(y) = \frac{3}{2\pi^2}\int_0^\infty x^2\, dx\, \sinh^{-2}\left(\frac{1}{2}\sqrt{x^2+y^2}\right), \tag{A.14}$$

and

$$f_{\text{fermi}}(y) = \frac{3}{2\pi^2}\int_0^\infty x^2\, dx\, \cosh^{-2}\left(\frac{1}{2}\sqrt{x^2+y^2}\right). \tag{A.15}$$

As $m_q/T \to 0$, the functions f_{bose} and f_{fermi} approach 2 and 1 respectively.

JHEP07(2010)056

References

[1] J.M. Maldacena, *The large-N limit of superconformal field theories and supergravity*, *Adv. Theor. Math. Phys.* **2** (1998) 231 [*Int. J. Theor. Phys.* **38** (1999) 1113] [hep-th/9711200] [SPIRES].

[2] E. Witten, *Anti-de Sitter space, thermal phase transition, and confinement in gauge theories*, *Adv. Theor. Math. Phys.* **2** (1998) 505 [hep-th/9803131] [SPIRES].

[3] E. Witten, *Anti-de Sitter space and holography*, *Adv. Theor. Math. Phys.* **2** (1998) 253 [hep-th/9802150] [SPIRES].

[4] S.S. Gubser, *Thermodynamics of spinning D3-branes*, *Nucl. Phys.* **B 551** (1999) 667 [hep-th/9810225] [SPIRES].

[5] K. Behrndt, M. Cvetič and W.A. Sabra, *Non-extreme black holes of five dimensional $N = 2$ AdS supergravity*, *Nucl. Phys.* **B 553** (1999) 317 [hep-th/9810227] [SPIRES].

[6] A. Chamblin, R. Emparan, C.V. Johnson and R.C. Myers, *Charged AdS black holes and catastrophic holography*, *Phys. Rev.* **D 60** (1999) 064018 [hep-th/9902170] [SPIRES].

[7] M. Cvetič and S.S. Gubser, *Phases of R-charged black holes, spinning branes and strongly coupled gauge theories*, *JHEP* **04** (1999) 024 [hep-th/9902195] [SPIRES].

[8] B. Sundborg, *The Hagedorn transition, deconfinement and $N = 4$ SYM theory*, *Nucl. Phys.* **B 573** (2000) 349 [hep-th/9908001] [SPIRES].

[9] O. Aharony, J. Marsano, S. Minwalla, K. Papadodimas and M. Van Raamsdonk, *The Hagedorn/deconfinement phase transition in weakly coupled large-N gauge theories*, *Adv. Theor. Math. Phys.* **8** (2004) 603 [hep-th/0310285] [SPIRES].

[10] D. Yamada and L.G. Yaffe, *Phase diagram of $N = 4$ super-Yang-Mills theory with R-symmetry chemical potentials*, *JHEP* **09** (2006) 027 [hep-th/0602074] [SPIRES].

[11] D. Yamada, *Metastability of R-charged black holes*, *Class. Quant. Grav.* **24** (2007) 3347 [hep-th/0701254] [SPIRES].

[12] T.J. Hollowood, S.P. Kumar, A. Naqvi and P. Wild, *$N = 4$ SYM on S^3 with near critical chemical potentials*, *JHEP* **08** (2008) 046 [arXiv:0803.2822] [SPIRES].

[13] A. Karch and L. Randall, *Open and closed string interpretation of SUSY CFT's on branes with boundaries*, *JHEP* **06** (2001) 063 [hep-th/0105132] [SPIRES].

[14] A. Karch and E. Katz, *Adding flavor to AdS/CFT*, *JHEP* **06** (2002) 043 [hep-th/0205236] [SPIRES].

[15] T. Sakai and S. Sugimoto, *Low energy hadron physics in holographic QCD*, *Prog. Theor. Phys.* **113** (2005) 843 [hep-th/0412141] [SPIRES].

[16] J. Babington, J. Erdmenger, N.J. Evans, Z. Guralnik and I. Kirsch, *Chiral symmetry breaking and pions in non-supersymmetric gauge/gravity duals*, *Phys. Rev.* **D 69** (2004) 066007 [hep-th/0306018] [SPIRES].

[17] I. Kirsch, *Generalizations of the AdS/CFT correspondence*, *Fortsch. Phys.* **52** (2004) 727 [hep-th/0406274] [SPIRES].

[18] K. Ghoroku, T. Sakaguchi, N. Uekusa and M. Yahiro, *Flavor quark at high temperature from a holographic model*, *Phys. Rev.* **D 71** (2005) 106002 [hep-th/0502088] [SPIRES].

[19] D. Mateos, R.C. Myers and R.M. Thomson, *Holographic phase transitions with fundamental matter*, *Phys. Rev. Lett.* **97** (2006) 091601 [hep-th/0605046] [SPIRES].

JHEP07(2010)056

[20] T. Albash, V.G. Filev, C.V. Johnson and A. Kundu, *A topology-changing phase transition and the dynamics of flavour*, *Phys. Rev.* **D 77** (2008) 066004 [hep-th/0605088] [SPIRES].

[21] A. Karch and A. O'Bannon, *Chiral transition of $N = 4$ super Yang-Mills with flavor on a 3-sphere*, *Phys. Rev.* **D 74** (2006) 085033 [hep-th/0605120] [SPIRES].

[22] S. Kobayashi, D. Mateos, S. Matsuura, R.C. Myers and R.M. Thomson, *Holographic phase transitions at finite baryon density*, *JHEP* **02** (2007) 016 [hep-th/0611099] [SPIRES].

[23] K. Ghoroku, M. Ishihara and A. Nakamura, *$D3/D7$ holographic gauge theory and chemical potential*, *Phys. Rev.* **D 76** (2007) 124006 [arXiv:0708.3706] [SPIRES].

[24] D. Mateos, R.C. Myers and R.M. Thomson, *Thermodynamics of the brane*, *JHEP* **05** (2007) 067 [hep-th/0701132] [SPIRES].

[25] S. Nakamura, Y. Seo, S.-J. Sin and K.P. Yogendran, *Baryon-charge chemical potential in AdS/CFT*, *Prog. Theor. Phys.* **120** (2008) 51 [arXiv:0708.2818] [SPIRES].

[26] A. Karch and A. O'Bannon, *Holographic thermodynamics at finite baryon density: some exact results*, *JHEP* **11** (2007) 074 [arXiv:0709.0570] [SPIRES].

[27] D. Mateos, S. Matsuura, R.C. Myers and R.M. Thomson, *Holographic phase transitions at finite chemical potential*, *JHEP* **11** (2007) 085 [arXiv:0709.1225] [SPIRES].

[28] O. Aharony, J. Sonnenschein and S. Yankielowicz, *A holographic model of deconfinement and chiral symmetry restoration*, *Annals Phys.* **322** (2007) 1420 [hep-th/0604161] [SPIRES].

[29] N. Horigome and Y. Tanii, *Holographic chiral phase transition with chemical potential*, *JHEP* **01** (2007) 072 [hep-th/0608198] [SPIRES].

[30] A. Roberge and N. Weiss, *Gauge theories with imaginary chemical potential and the phases of QCD*, *Nucl. Phys.* **B 275** (1986) 734 [SPIRES].

[31] M. Kruczenski, D. Mateos, R.C. Myers and D.J. Winters, *Meson spectroscopy in AdS/CFT with flavour*, *JHEP* **07** (2003) 049 [hep-th/0304032] [SPIRES].

[32] A. O'Bannon, *Holographic thermodynamics and transport of flavor fields*, arXiv:0808.1115 [SPIRES].

[33] C. DeTar and U.M. Heller, *QCD thermodynamics from the lattice*, *Eur. Phys. J.* **A 41** (2009) 405 [arXiv:0905.2949] [SPIRES].

[34] P. de Forcrand, *Simulating QCD at finite density*, PoS(LAT2009)010 [arXiv:1005.0539] [SPIRES].

[35] P. de Forcrand and O. Philipsen, *The QCD phase diagram for small densities from imaginary chemical potential*, *Nucl. Phys.* **B 642** (2002) 290 [hep-lat/0205016] [SPIRES].

[36] P. de Forcrand and O. Philipsen, *The QCD phase diagram for three degenerate flavors and small baryon density*, *Nucl. Phys.* **B 673** (2003) 170 [hep-lat/0307020] [SPIRES].

[37] P. de Forcrand and O. Philipsen, *The chiral critical line of $N_f = 2 + 1$ QCD at zero and non-zero baryon density*, *JHEP* **01** (2007) 077 [hep-lat/0607017] [SPIRES].

[38] P. de Forcrand and O. Philipsen, *Constraining the QCD phase diagram by tricritical lines at imaginary chemical potential*, arXiv:1004.3144 [SPIRES].

[39] M. D'Elia and M.-P. Lombardo, *Finite density QCD via imaginary chemical potential*, *Phys. Rev.* **D 67** (2003) 014505 [hep-lat/0209146] [SPIRES].

[40] M. D'Elia and M.P. Lombardo, *QCD thermodynamics from an imaginary mu(B): Results on the four flavor lattice model*, *Phys. Rev.* **D 70** (2004) 074509 [hep-lat/0406012] [SPIRES].

JHEP07(2010)056

[41] M. D'Elia, F. Di Renzo and M.P. Lombardo, *The strongly interacting Quark Gluon Plasma and the critical behaviour of QCD at imaginary chemical potential*, *Phys. Rev.* **D 76** (2007) 114509 [arXiv:0705.3814] [SPIRES].

[42] M. D'Elia and F. Sanfilippo, *Thermodynamics of two flavor QCD from imaginary chemical potentials*, *Phys. Rev.* **D 80** (2009) 014502 [arXiv:0904.1400] [SPIRES].

[43] M. D'Elia and F. Sanfilippo, *The order of the Roberge-Weiss endpoint (finite size transition) in QCD*, *Phys. Rev.* **D 80** (2009) 111501 [arXiv:0909.0254] [SPIRES].

[44] P. Cea, L. Cosmai, M. D'Elia and A. Papa, *The phase diagram of QCD with four degenerate quarks*, arXiv:1004.0184 [SPIRES].

[45] A. Roberge and N. Weiss, *Gauge theories with imaginary chemical potential and the phases of QCD*, *Nucl. Phys.* **B 275** (1986) 734 [SPIRES].

[46] J. Braun, L.M. Haas, F. Marhauser and J.M. Pawlowski, *On the relation of quark confinement and chiral symmetry breaking*, arXiv:0908.0008 [SPIRES].

[47] M. Bluhm and B. Kampfer, *Quasiparticle model of quark-gluon plasma at imaginary chemical potential*, *Phys. Rev.* **D 77** (2008) 034004 [arXiv:0711.0590] [SPIRES].

[48] Y. Sakai, K. Kashiwa, H. Kouno and M. Yahiro, *Phase diagram in the imaginary chemical potential region and extended Z3 symmetry*, *Phys. Rev.* **D 78** (2008) 036001 [arXiv:0803.1902] [SPIRES].

[49] K. Kashiwa, M. Matsuzaki, H. Kouno, Y. Sakai and M. Yahiro, *Meson mass at real and imaginary chemical potentials*, *Phys. Rev.* **D 79** (2009) 076008 [arXiv:0812.4747] [SPIRES].

[50] H. Kouno, Y. Sakai, K. Kashiwa and M. Yahiro, *Roberge-Weiss phase transition and its endpoint*, *J. Phys.* **G 36** (2009) 115010 [arXiv:0904.0925] [SPIRES].

[51] N. Weiss, *The effective potential for the order parameter of gauge theories at finite temperature*, *Phys. Rev.* **D 24** (1981) 475 [SPIRES].

[52] N. Weiss, *The Wilson line in finite temperature gauge theories*, *Phys. Rev.* **D 25** (1982) 2667 [SPIRES].

[53] C. Fefferman and C. Robin Graham, *Conformal invariants*, in *Élie Cartan et les Mathématiques d'aurjourd'hui*, *Asterique* **95** (1985).

[54] A. Karch, A. O'Bannon and K. Skenderis, *Holographic renormalization of probe D-branes in AdS/CFT*, *JHEP* **04** (2006) 015 [hep-th/0512125] [SPIRES].

[55] O. Aharony and E. Witten, *Anti-de Sitter space and the center of the gauge group*, *JHEP* **11** (1998) 018 [hep-th/9807205] [SPIRES].

[56] J.M. Maldacena, *Wilson loops in large-N field theories*, *Phys. Rev. Lett.* **80** (1998) 4859 [hep-th/9803002] [SPIRES].

[57] S.-J. Rey and J.-T. Yee, *Macroscopic strings as heavy quarks in large-N gauge theory and anti-de Sitter supergravity*, *Eur. Phys. J.* **C 22** (2001) 379 [hep-th/9803001] [SPIRES].

[58] H.-U. Yee, *Fate of $Z(N)$ domain wall in hot holographic QCD*, *JHEP* **04** (2009) 029 [arXiv:0901.0705] [SPIRES].

[59] R.C. Myers, A.O. Starinets and R.M. Thomson, *Holographic spectral functions and diffusion constants for fundamental matter*, *JHEP* **11** (2007) 091 [arXiv:0706.0162] [SPIRES].

[60] C. Hoyos-Badajoz, K. Landsteiner and S. Montero, *Holographic meson melting*, *JHEP* **04** (2007) 031 [hep-th/0612169] [SPIRES].

[61] T. Faulkner and H. Liu, *Condensed matter physics of a strongly coupled gauge theory with quarks: some novel features of the phase diagram*, arXiv:0812.4278 [SPIRES].

JHEP07(2010)056

[62] T. Faulkner and H. Liu, *Meson widths from string worldsheet instantons*, *Phys. Lett.* **B 673** (2009) 161 [arXiv:0807.0063] [SPIRES].

[63] P. Benincasa, *Universality of holographic phase transitions and holographic quantum liquids*, arXiv:0911.0075 [SPIRES].

[64] T. Hollowood, S.P. Kumar and A. Naqvi, *Instabilities of the small black hole: a view from* $N = 4$ *SYM*, *JHEP* **01** (2007) 001 [hep-th/0607111] [SPIRES].

JHEP07(2010)056